Absorption of aerosols above clouds from POLDER/PARASOL measurements and estimation of their Direct Radiative Effect

F. Peers[1], F. Waquet[1], C. Cornet[1], P. Dubuisson[1], F. Ducos[1], P. Goloub[1], F. Szczap[2], D. Tanré[1], F. Thieuleux[1]

[1]{Laboratoire d'Optique Atmosphérique, Université Lille 1, Villeneuve d'Ascq, France}

[2]{Laboratoire de Météorologie Physique, Clermont-Ferrand, France}

Correspondence to: F. Peers (fanny.peers@ed.univ-lille1.fr) and F. Waquet (fabien.waquet@univ-lille1.fr)

Abstract

This study presents an original method to evaluate key parameters for the estimation of the direct radiative effect of aerosol above clouds: the absorption of the aerosol layer and the albedo of the underneath cloud. It is based on multi-angle total and polarized radiances both provided by the A-train satellite instrument POLDER - Polarization and Directionality of Earth Reflectances. The sensitivities brought by each kind of measurements are used in a complementary way. Polarization mostly translates scattering processes and is thus used to estimate the scattering aerosol optical thickness and the aerosol size. On the other hand, total radiances, together with the scattering properties of aerosols, are used to evaluate the absorption optical thickness of aerosols and the cloud optical thickness. The retrieval of aerosol and clouds properties (i.e. aerosol and cloud optical thickness, aerosol single scattering albedo and angström exponent) is restricted to homogeneous and optically thick clouds (cloud optical thickness larger than 3). In addition, a procedure has been developed to process the shortwave direct radiative effect of aerosols above clouds. Three case studies have been selected: a case of absorbing biomass burning aerosols above clouds over the South-East Atlantic Ocean, a Siberian biomass burning event and a layer of Saharan dust above clouds off the North-West African coast. Besides these case studies (i.e. biomass burning aerosols from Africa and Siberia and Saharan dust), both algorithms have been applied on the South East Atlantic Ocean and results have been averaged through August 2006. The mean direct radiative effect is found to be 33.5 $W.m^{-2}$ (warming). Finally, the effect of the heterogeneity

of clouds has been investigated and reveals that it affects mostly the retrieval of the cloud optical thickness and not much the aerosols properties. The homogenous cloud assumption used in both the properties retrieval and the DRE processing leads to a slight underestimation of the DRE.

1. Introduction

The quantification of the aerosol radiative impact is one of the largest sources of uncertainty in global climate models [Myhre et al., 2013b]. These uncertainties are mainly related to aerosols in cloudy scenes through direct, semi-direct and indirect effects. The last two describe the modifications of cloud microphysics because of interactions between clouds and aerosols [Bréon et al., 2002]. Especially, the enhancement of the number of cloud condensation nuclei results in a reduction of cloud droplet size, leading in an enhancement of the cloud albedo [Twomey, 1974 & 1977], a prolongation of their lifetime and a decrease of precipitation [Albrecht, 1989; Ramanathan et al., 2001]. The semi-direct effect refers to changes in cloud formation attributable to the aerosol influences on the vertical stability of the atmosphere [Ackerman et al., 2000; Johnson et al., 2004; Koren et al., 2004; Kaufman et al, 2005]. Finally, the direct effect corresponds to the modification of the amount of solar radiation scattered back to space by the clouds due to the presence of an aerosol layer. Figure 1 illustrates the difference of albedo of a scene $\Delta\rho$ caused by an aerosol layer versus the albedo of the underneath surface. It has been calculated using the approximate expression given by Lenoble et al. [1982]:

$$\Delta\rho = \rho - \rho_s = \tau(\varpi_0(1-g)(1-\rho_s)^2 - 4(1-\varpi_0)\rho_s) \quad (1)$$

ρ_s being the clean-sky albedo of the scene, and ρ, the albedo with aerosols. The aerosol optical thickness τ is related to the amount of particles and corresponds to the sum of the absorption optical thickness τ_{abs} and the scattering one τ_{scatt}. The Single Scattering Albedo (SSA) ϖ_0 describes the relative contribution of the aerosol scattering to the extinction (i.e. scattering and absorption, $\varpi_0 = \tau_{scatt}/\tau$). Finally, the aerosol asymmetry factor g characterizes the preferential direction of the scattered light. The difference of albedo and the shortwave Direct Radiative Effect (DRE) of aerosols are directly proportional. A positive difference of albedo means that the scene appears brighter with aerosols (domination of the scattering process) and thus, it results in a cooling effect (DRE<0). This is the case for aerosols above a dark surface as, for instance, over ocean. Over a bright scene such as clouds, the sign of the difference of albedo strongly depends on the absorption of the aerosol layer (i.e. the single scattering

albedo): absorbing aerosols can lead to a darkening (warming effect), but for particles which would scatter enough, the resulting forcing can be positive (cooling effect). As a consequence, the improvement of the DRE estimation is driven by the accurate knowledge of the albedo of the underneath surface, the amount of aerosols and their level of absorption.

In order to constrain numerical models, satellite aerosol retrievals provide essential information on aerosol and cloud properties, spatial distribution and trends. However, the study of aerosol layer above clouds is a recent line of research and the radiative effects of aerosols located above clouds remain unconstrained because most current satellite retrievals are limited to cloud-free scenes. In addition, the retrieval of cloud properties that determine the cloud albedo (i.e. the cloud optical thickness and the droplet effective radius) is impacted by the presence of an aerosol layer above [Haywood et al., 2004; Wilcox et al., 2009; Coddington et al., 2010] and consequently, it biases the estimation of the DRE. Active sensors like the Cloud-Aerosol Lidar with Orthogonal Polarization (CALIOP) are dedicated to the analysis of the atmospheric vertical profile. An operational algorithm [Winker et al., 2009 & 2013; Young and Vaughan, 2009] as well as two alternative research methods (i.e. the de-polarization ratio [Hu et al., 2007] and the color-ratio method [Chand et al., 2008]) enable the retrieval of the Above Clouds Aerosols Optical Thickness (ACAOT). Nevertheless, passive sensors have also shown an ability to extract information from Above Clouds Aerosols (ACA) measurements and gain advantage from their wide spatial coverage. Based on the capacity of aerosols to absorb the UV radiations reflected by the clouds, Torres et al. [2012] have developed a method to calculate the UV aerosol index and, under some assumption on the aerosol properties, to retrieve the ACAOT as well as the Aerosol-Corrected Cloud Optical Thickness (ACCOT) with Ozone Monitoring Instrument (OMI). The amount of particles above clouds and the ACCOT can also be retrieved simultaneously using measurements in the visible and in the shortwave infrared from the Moderate Resolution Imaging Spectroradiometer (MODIS), thanks to the color-ratio method developed by Jethva et al. [2013].

Contrary to total radiances, polarized measurements are primarily sensitive to the single scattering process and does no longer depend on the optical thickness of the cloud when it is thick enough. Waquet et al. [2009 & 2013a] have developed a method to retrieve the ACAOT at two wavelengths and therefore the angstrom exponent, using polarized radiances from the Polarization and Directionality of Earth Reflectances (POLDER). Jethva et al. [2014] have carried out a multi-sensor comparison of the above-cloud AOT retrieved from different

sensors on board NASA's A-train satellite for a biomass burning event off the South West African coast. Considering the different kinds of assumptions and measurements used to retrieve the ACAOT, results have shown good consistency over the homogeneous cloud fields. Since aerosol and cloud properties are known, it is possible to process the DRE of aerosols above clouds with a radiative transfer model [Chand et al., 2009; Peters et al., 2011; Costantino and Bréon, 2013; Meyer et al., 2013]. However, most of the ACAOT retrievals presented above do not evaluate the aerosol single scattering albedo. In contrast, the DRE of aerosols above clouds can also be evaluated without making assumptions on aerosol microphysics thanks to the algorithm developed by De Graaf et al. [2012] for Scanning Imaging Absorption Spectrometer for Atmospheric Chartography (SCIAMACHY) measurements. Hyperspectral reflectances from polluted cloud scenes are converted into flux and subtract from the clean cloud one. The latter is modeled thanks to cloud properties derived from SCIAMACHY measurements in the short wave infrared spectrum. While this method is expected to work efficiently for fine mode aerosols as their interactions at longer wavelengths are minimal or even nil, it may not work for coarse mode dust aerosols due to their radiative influence at longer wavelengths.

All those retrievals methods have shown that both total and polarized radiances are sensitive to ACA in the scene. The POLDER instrument on PARASOL satellite has the advantage to measure both for several viewing angles and wavelengths [Tanré et al., 2011]. In the next section of this paper, we will evaluate the contribution brought by the combination of the scattering information provided by polarization and the absorption one given by total radiances. We will explore an improved retrieval method for ACA scenes over ocean based on the work of Waquet et al. [2013a] for the three main parameters required to estimate the DRE: the ACAOT, the ACCOT and the SSA of ACA. The previous algorithm has already demonstrated its ability to detect different kinds of particles (i.e. biomass burning, pollution and dust) over clouds at global scale [Waquet et al., 2013b]. In the third section, we will present a module for the processing of ACA DRE. Beyond their types, aerosol absorption properties are expected to vary a lot depending on space, time and formation processes [Dubovik et al., 2002] and thus, resulting on different radiative responses. Both algorithms have been applied to three events with contrasted aerosol properties: absorbing biomass burning aerosols off the South West coast of Africa, scattering ones from Siberia and Saharan dust. Then, aerosol and cloud properties as well as the DRE have been evaluated and averaged through August 2006 over the South East Atlantic Ocean. This region is a key area

for the study of aerosol impacts in cloudy skies since biomass burning particles from Africa are usually transported westward over clouds during the dry season. The case studies and the monthly results will be shown in the section 4. Thereafter, the impact of cloud heterogeneity on our estimation of ACA parameters and the DRE will be examined in section 5. Conclusion will be drawn in section 6.

2. Retrieval method

2.1. Description

Polarized measurements can be used to extract information from ACA scenes [Waquet et al., 2009 & 2013a; Hasekamp, 2010; Knobelspiesse et al., 2011] owing to the specific signal produced by cloud liquid droplets. Figure 2 illustrates polarized radiances processed with the SOS code [Deuzé et al., 1989] for a cloudy atmosphere, with (colored lines) and without aerosols above (black line). It should be noted that, in this paper, the radiance refers to the normalized quantity according to the definition given by Herman et al. [2005]. Regarding the clean cloud signal, the amount of polarized light generated by the cloud is very weak at side scattering angles (70° - 130°). Also, it does not depend on the COT as long as it is larger than 3.0. The aerosol model used for the polluted cloud cases corresponds to fine mode particles with an effective radius of 0.10 µm. The scattering AOT is fixed (i.e. $AOT_{scatt} = 0.18$) while the level of absorption (i.e. AOT_{abs}) has been stretched through the complex part of the refractive index k. The scattering of light by fine mode aerosols causes the creation of an additional polarized signal at side scattering angles. Moreover, in accordance to the sensitivity analysis performed by Waquet et al. [2013a], the effect of absorption processes on polarization is weak for any scattering angles lower than 130°. Thus, the signal is mostly attributable to scattering processes. At the same time, cloud water droplets produce a large peak of polarization at about 140° that is strongly attenuated by aerosols for ACA events. These two effects can be used to derive aerosol scattering properties from multidirectional polarized measurements like the ones provided by POLDER.

In case of clean sky condition (i.e. without aerosols), the total radiances scattered by cloud water droplets are relatively spectrally independent from the UV to the Short Wave InfraRed (SWIR) part of the spectrum [De Graaf et al., 2012]. At the same time, those wavelengths are sensitive to aerosol effects (i.e. absorption and scattering) whose spectral behaviors depend strongly on the microphysics of the particles (e.g. size, chemical composition, shape).

Consequently, the presence of an aerosol layer above clouds affects the signal that can be measured by satellite instruments: the spectral tendency of aerosol absorption leads to a modification of the apparent color of the clouds. Simulations of the upwelling radiance at 490 and 865 nm for ACA events have been processed with a radiative transfer code based on the adding-doubling method [De Haan et al., 1987]. In the same way as Fig. 3 in the study of Jethva et al. [2013], Fig. 3 highlights the color ratio effect. The radiance ratio (L_{490}/L_{865}) is plotted against the SWIR radiance (L_{865}) for several Cloud Optical Thicknesses (COT) and for aerosols with an effective radius of 0.1 µm. Similarly to the previous figure, the scattering AOT is fixed and several absorption AOT is considered. The complex part of the refractive index *k* is set equal at both wavelengths. This plot clearly illustrates the enhancement of the spectral contrast with absorption. For a given value of the radiance ratio, the 865 nm band provides the sensitivity to the COT. That is to say, radiances at 490 and 865 nm can be interpreted as a coupled ACCOT and absorption ACAOT as long as the scattering optical thickness of aerosol and their size are known.

2.2. POLDER data

The POLDER instrument is the main part of the PARASOL's payload (Polarization and Anisotropy of Reflectances for Atmospheric Science coupled with Observations from a Lidar) that have flown from 2004 to 2013, including 5 years as a part of the A-train constellation. It provides radiances for 9 spectral bands between 443 and 1020 nm as well as polarization measurements over 3 (i.e. 490, 670 and 865 nm). Thanks to its 2-dimensional CCD camera, the instrument acquires a series of images, which allow the target to be seen from up to 16 viewing angles. The ground spatial resolution of POLDER at nadir is 5.3x6.2 km^2. A new version of Level 1 (v03.02) products will be released by the CNES by the end of 2014 including an improvement of the radiometric calibration [Fougnie et al., 2007]. Meanwhile, the data used in this paper corresponds to the previous version (i.e. PARASOL Collection 2 v02.04).

2.3. Algorithm

The distinctive feature of the method presented here is to combine the information provided by both total and polarized multidirectional radiances from POLDER. The first step consists in estimating the scattering optical thickness and the aerosol size with polarization. We proceed with the Look Up Table (LUT) approach described by Waquet et al. [2013a].

Polarized radiances at 670 and 865 nm have been computed with the SOS code [Deuzé et al., 1989] for seven models of aerosols that follow a lognormal size distribution (cf. Table 1). Six of them correspond to spherical aerosols from the fine mode with radius from 0.06 to 0.16 µm and assuming a complex refractive index of $1.47 - 0.01i$. The last one is a nonspherical model for dust with a refractive index of $1.47 - 0.0007i$. The retrieval of the scattering AOT is attempted for each 6km × 6km POLDER's pixel when the COT given by MODIS is larger than 3.0. If fine mode aerosols have been identified, the estimation of the scattering AOT is based on the polarized signal measured for scattering angle lower than 130°. At that point, a first estimation of the extinction AOT is made based on the absorption assumed for the selected aerosol model (i.e. $k_{assumption}$). Results are then subjected to several filters in order to improve their quality: data must be well fitted, clouds have to be homogeneous and both cloud edges and cirrus are rejected according to criteria based on POLDER and MODIS products. Filtered AOT are then aggregated from 6 km × 6 km to 18 km × 18 km and pixels with a Standard Deviation (SD) of the AOT larger than 0.1 are excluded in order to prevent cloud edge contamination. Eventually, the scattering AOT is recovered using the SSA of the aerosol model with the same absorption assumption used at first (i.e. $k_{assumption}$):

$$\tau_{scatt,\lambda} = \varpi_{0,\lambda,k_{assumption}} \tau_{ext,\lambda,k_{assumption}} \quad (2)$$

τ_{scatt} being the scattering AOT, τ_{ext} the extinction AOT retrieved with polarization, ϖ_0 the SSA corresponding to the model used for the retrieval and λ referring to the wavelength. We consider that the aerosol size corresponds to the one of the model with the nearest model (i.e. not interpolated).

The second part of the method aims at evaluating the absorption of ACA and the ACCOT using multidirectional radiances at 490 and 865 nm and the information on properties already provided by polarization. Once again, the process consists in a comparison with radiance LUT. For computing time reason, we have chosen to process radiances with the adding-doubling code [De Haan et al., 1987] instead of the one used for the polarized LUT (i.e. SOS code). The models are based on the 7 ones previously considered with several imaginary parts of the refractive index k (cf. Table 1). For the fine mode, k varies from 0.00 to 0.05 and it is assumed to be the same at both wavelengths because only a weak variation of this parameter is expected between the used bands for this type of aerosols. On the opposite, the dust complex part of the refractive index should have a pronounced spectral dependence because of the presence of iron oxide that absorbs blue and UV radiation. Consequently, we have set the value of k to 0.0007 at 865 nm, based on the result obtained with the research algorithm

developed in Waquet et al. [2013a]. The absorption at 490 nm is evaluated in a range of k from 0.000 to 0.004. Considering cloud properties (cf. Table 1), the droplet effective size distribution is considered to follow a gamma law with an effective variance of 0.06. The cloud droplet effective radius is set to 10.0 µm since the wavelengths selected for the retrieval do not have a noticeable sensitivity to this parameter [Rossow et al., 1989]. The cloud top height is fixed at 1 km and the aerosol layer is located between 2 and 3 km. Finally, the reflection of the solar radiation by the ocean surface (i.e. the sunglint), which can be significant for optically thin clouds, is taking into account by considering surface wind speed from 2.0 to 15.0 $m.s^{-1}$ [Cox and Munk, 1954]. The input data are the multidirectional radiances at 490 and 865 nm from 6x6 km^2 from POLDER (i.e. the whole directional information is used), the scattering ACAOT and the aerosol model previously determined and the surface wind speed from modeling. The retained solution is the one that minimizes the least square error term ε:

$$\varepsilon = \sum_{i=1}^{N_\Theta} \sum_{j=1}^{N_\lambda} \left[L_{ij}^{meas}(\Theta) - L_{ij}^{calc}(\Theta) \right]^2 \quad (3)$$

L referring to measured (*meas*) and calculated (*calc*) radiances and Θ being the scattering angle. In accordance with the operational product of POLDER clear-sky retrieval, the angström exponent α is calculated from the optical thicknesses τ at 670 and 865 nm using the expression below:

$$\alpha = -\frac{\log\left(\tau_{670\,nm} / \tau_{865\,nm}\right)}{\log\left(670.0 / 865.0\right)} \quad (4)$$

An example of total radiances measured at 490 and 865 nm by POLDER for one pixel is given in Fig. 4a and 4b respectively. The estimation of the cloud and aerosol properties has been derived thanks to the method described hereinbefore. Aerosols belong to the fine mode with an ACAOT of 0.142 at 865 nm and a complex part of the refractive index k at 0.035. The COT is evaluated at 12.4. Figure 4 also illustrates the signal modeled during the retrieval for different levels of absorption with an ACCOT corresponding to our solution. For completely scattering particles (i.e. $k = 0.00$), one can note that SWIR and visible radiances reach approximately the same levels. In that case, the scene appears almost spectrally neutral. When the absorption AOT is increased (i.e. increasing of the complex part of the refractive index k), both radiances decrease. However, one can notice the increasing gap between visible and SWIR radiances as the absorption grows called the color ratio effect. Since aerosol absorption

has a spectral signature, it produces stronger absorption effects at shorter wavelengths than at longer ones.

2.4. Sensitivity analysis

The method developed hereinbefore requires assumptions at different stages of the retrieval. The aim of this section is to analyze the resulting impact on the retrieval. To serve this purpose, POLDER's observations have been modeled with the same radiative transfer code used for the LUT, considering several aerosol and cloud models. These modeled signals have been used as inputs for the algorithm. It implies that errors due to the polarization part of the retrieval are investigated and then, impacted on the total radiances step.

We first examine the assumption regarding aerosol properties. In order to retrieve the scattering AOT, it is assumed that polarized measurements are weakly sensitive to aerosol absorption. This approximation is expected to become less consistent when the aerosol layer is very absorbing (i.e. large AOT and low SSA). This leads to an error in the estimation of the scattering AOT that could affect the retrieval of the SSA. The second assumption concerns the real part of the refractive index m fixed at 1.47 for the retrieval. To assess the impact of these assumptions, we have considered 3 absorbing aerosol models with different refractive indices n: $1.42 - 0.03i$, $1.47 - 0.03i$ and $1.52 - 0.03i$ corresponding to a SSA at 865 nm of 0.735, 0.772 and 0.801, respectively. The real parts of the refractive indices have been chosen to be representative of the variability observed within the aerosol fine mode [Dubovik et al., 2002]. Aerosols have an effective radius of 0.1µm and their mean altitude is 3 km. The cloud layer used to model the signal has a top altitude at 0.75 km, an optical thickness of 10 and a droplet effective radius of 10 µm. Total and polarized radiances have been simulated for absorbing aerosol layers with increasing AOT. Finally, the DRE of aerosols has been processed using the radiative transfer code GAME [Dubuisson et al, 2004], based on the properties of the modeled scene on the one hand, and those retrieved by the algorithm on the other hand. In Fig. 5, the aerosol and cloud parameters retrieved (green lines) and used in the reference states (i.e. input simulations - grey lines) are plotted as a function of the AOT at 865 nm. The middle column (i.e. $n = 1.47 - 0.03i$) shows the biases due to the approximation that polarized radiances translate the scattering process only while the left and the right ones (i.e. $n = 1.42 - 0.03i$ and $1.52 - 0.03i$) present also the effect due to the assumption on the real part of the refractive index.

- The first two rows display the total and the scattering AOT. For m = 1.42 and 1.47, the algorithm underestimates the AOT. This error comes from the underestimation of the scattering AOT during the polarized part of the retrieval. For AOT lower than 0.2, we observe a bias around 20% on the AOT. In case of extreme events, with AOT around 0.6 (i.e. 1.5 at 550 nm), the AOT is underestimated of 26.7% for m = 1.47 and 24.1% for m = 1.42, respectively. On the opposite, the algorithm overestimate the AOT when m = 1.52. It has to be noted that the retrieved aerosol radius is larger than the one use to model the signal (0.12 µm instead of 0.1 µm). In that case, the largest error on the AOT (i.e. 25.3%) is observed at AOT = 0.2. Then, the error slowly decreases with the AOT because of the compensation with the aerosol absorption, reaching 16.8% at AOT = 0.6.

- Rows 3 and 4 of Fig. 5 show the absorption AOT and the SSA versus the total AOT. In spite of the error on the scattering AOT, it is interesting to observe that the biases on the absorption AOT are small. Because of the sensitivity of total radiances to the absorption of the aerosol layer, the algorithm compensates the bias on the scattering AOT due to the first part by an error on the SSA. As a consequence, a negative error (resp. positive) in the scattering AOT goes together with an underestimation (resp. overestimation) of the SSA. For AOT = 0.6, a bias of −0.055 has been observed for m = 1.42 and 1.47 and +0.033 for m = 1.52, respectively.

- Plots of the 4th row represent the retrieved COT. They reveal that both the approximation regarding polarized radiance and the assumption on the real part of the refractive index have a limited impact on the COT estimation. In this analysis, the largest bias is ±0.3 on the COT.

- Finally, the last line focuses on the evolution of the DRE of aerosols with the modeled AOT. The DRE estimated with aerosol and cloud properties retrieved by the algorithm is close to the one processed with the properties of the modeled scene. This can be explained by the reliable estimation of the aerosol layer absorption: as suggested by Eq. (1), the absorption AOT is the leading parameter in the estimation of the DRE for large values of the albedo of the underneath scene. The largest bias (+9.7 W.m^{-2}) has been obtained for AOT = 0.6 and m = 1.52. Otherwise, the bias is always lower than ±6.4 W.m^{-2} for AOT lower than 0.2 and lower than ±1 W.m^{-2} for AOT lower than 0.1.

In a second place, we look at the assumption on the size distribution of the coarse mode particles. For the retrieval, we only consider one model for dust. It is defined by a bimodal lognormal size distribution with an angström exponent of 0.36 [Waquet et al., 2013a]. The

signal has been modeled for coarse mode particles with an angström exponent of 0.02 and 0.6 and an AOT = 0.6. The method appears to allow a consistent evaluation of the SSA at 490 nm (error < 1%) in spite of the error on the optical thickness and on the angström exponent (error on AOT around 24% and on angström exponent 100%).

The last assumption about aerosols that has been investigated concerns the vertical distribution of the aerosol layer. We have processed the signal for an aerosol top altitude of 4 and 6 km and the algorithm has retrieved the correct aerosol and cloud properties. In polarization, the bands used to retrieve the scattering AOT (i.e. 670 and 865 nm) are weakly impacted by the molecular contribution. Aerosols in the clouds do not contribute to the creation of polarized signal at side scattering angle. Hence the polarized radiances are not impacted by the aerosol vertical distribution as long as the aerosol layer is distinct from the cloud.

Regarding the cloud hypothesis, we test the impact of considering only one cloud droplet effective radius ($r_{\text{eff,cld}}$ = 10 µm) for the estimation of the aerosol absorption and the ACCOT by modeling the signal for $r_{\text{eff,cld}}$ = 6 and 20 µm with a COT = 10. The approximation regarding the effective radius of cloud droplet is the main source of error on the COT estimation. While the error on the COT due to aerosol hypothesis does not exceed 3%, this one may lead to a bias of ±10% for the COT, which is in agreement with the study of Rossow et al. [1989]. However, statistical analysis of the scenes studied hereafter have shown that more than 70% of the clouds have an effective radius ranging between 8 and 16 µm. Lastly, we have investigated the influence of the cloud top altitude by considering $z_{\text{top,cld}}$ = 2 and 4 km. For each case, the algorithm has retrieved the correct parameters for clouds and aerosols.

3. Radiative Effect Estimation

As previously shown, the accurate knowledge of the aerosol and cloud properties is required for estimating the direct radiative forcing due to an aerosol layer above clouds. At the Top Of the Atmosphere (TOA), this instantaneous Direct Radiative Effect (DRE) $\Delta F(\theta_s)$ is expressed as a flux difference given by:

$$\begin{aligned}\Delta F(\theta_s) &= \left(F^{\downarrow}(\theta_s) - F^{\uparrow}_{cloud+aer}(\theta_s)\right) - \left(F^{\downarrow}(\theta_s) - F^{\uparrow}_{cloud}(\theta_s)\right) \\ &= F^{\uparrow}_{cloud}(\theta_s) - F^{\uparrow}_{cloud+aer}(\theta_s)\end{aligned} \quad (5)$$

θ_s being the solar zenith angle, $F^{\downarrow}$ the downward flux at the TOA, $F^{\uparrow}_{cloud+aer}$ the upward flux when aerosols are present and $F^{\uparrow}_{cloud}$ corresponds to the flux reflected by clouds with no aerosol above.

Since the approximate method described earlier (Eq. (1)) could lead to results not correct enough for coarse mode particles, we have chosen to found our approach on exact calculation based on the radiative transfer code GAME [Dubuisson et al, 2004]. Instantaneous shortwave radiative forcing (i.e. from 0.2 to 4 µm) has been precomputed for several solar zenith angles. Regarding fine mode aerosols, they are assumed to be only composed of black carbon. In other words, the imaginary part of the refractive index is constant in the shortwave (grey aerosols) and corresponds to the one retrieved by our algorithm. For dust aerosols, the spectral dependence of the absorption is based on the work of Balkanski et al. [2007], adjusting the UV imaginary part of the refractive index with the retrieved value at 490 nm. In addition to the aerosol and cloud properties derived using the methods described hereinbefore (i.e. ACCOT, ACAOT, the aerosol size and their absorption), the LUT takes into account several cloud droplet effective radii and atmospheric vertical distributions. Those latest are characterized by the cloud top height (considering an aerosol layer between 1 and 2 km above the cloud), the amount of absorbing gases (i.e. ozone and water vapor) and the atmospheric model (i.e. the pressure, temperature and gases vertical profiles). The DRE is obtained by interpolation of the LUT.

Regarding the additional input data, the information about the cloud droplets size comes from MODIS [Nakajima and King, 1990]. The cloud top height is derived from the POLDER apparent O2 cloud top pressure [Vanbauce et al., 2003] since the O2 retrieval allows a reliable estimation of the cloud top height in the presence of an aerosol layer above [Waquet et al., 2009]. The ozone and water vapor contents are given by meteorological modeling. Finally, the atmospheric vertical profile depends on the seasons and the geographic location [Cole et al., 1965] (i.e. mid-latitude, tropical, sub-arctic summer and winter).

4. Results

4.1. Case studies

The RGB images of the 3 selected case studies are shown in Fig. 6. The first one (Fig. 6a) is related to a biomass burning event during the dry season in the South of Africa, the second (Fig. 6b) concerns Siberian biomass burning aerosols transported above clouds, and the last

one (Fig. 6c) is about Saharan dust. For each case, the retrieved parameters (i.e. the ACAOT, the aerosol scattering albedo, their angström exponent and the ACCOT) will be shown as well as the estimation of the DRE.

4.1.1. African biomass burning aerosols

From June to October, biomass burning particles from man made vegetation fires are frequently observed above the persistent deck of stratocumulus covers off the South West African coast. On 4th August 2008 (Fig. 6a), biomass burning aerosols have been observed over clouds. Under the CALIOP track (not shown), the aerosol layer is located between 3 and 5 km and the cloud top at 1 km.

The evaluation of aerosol and cloud properties has been performed over ocean and results are displayed in Fig. 7. The ACAOT (Fig. 7a) reach high values up to 0.74 at 865 nm. As expected, aerosols are found to belong to the fine mode with effective radius, from 0.10 µm close to the coast, to 0.16 µm as the plume shifts to the open sea. The angström exponent (Fig. 7b), which depends not only on the aerosol size but also slightly on the refractive index, is around 1.94. Figure 7c shows the low values obtained for the SSA expressing the strong absorbing capability of these aerosols. The lowest SSAs are about 0.73 at 865 nm near the coast. These aerosols are associated with a complex part of the refractive index around 0.042. The average SSA of the scene is of 0.875 and 0.840 at 550 and 865 nm, respectively, which is consistent with previous African savannah biomass burning retrieval from AERONET [Dubovik et al., 2002; Sayer et al. 2014] and remote and in-situ measurements from the SAFARI 2000 campaign [Leahy et al., 2007; Johnson et al., 2008].

The retrieved ACCOT as well as the difference with MODIS observations are shown in Fig. 7d and 7e. The pattern followed by the ACCOT is close to the one given by MODIS. However, the comparison between the two methods reveals systematic biases when absorbing aerosols are above clouds. According to previous studies [Haywood et al., 2004; Wilcox et al., 2009; Coddington et al., 2010; Meyer et al., 2013; Jethva et al., 2013], the estimation of the COT that takes into account the aerosol absorption gives higher values than the MODIS MYD06 cloud product. Because aerosols absorb at the wavelengths traditionally use to retrieve the COT, the cloud appears darker leading to an underestimation of its optical thickness. The impact of the aerosol absorption on the signal gets bigger as the COT increases. Where the clouds are the thickest and the absorption ACAOT the largest (i.e. a

small area around (10°S, 8°E)), the bias is around 15. On average over the whole scene, ACCOT is larger than the MODIS value by 1.2.

Finally, the DRE has been estimated and is reported in Fig. 7f. As expected for highly absorbing aerosols, the warming effect reaches high level with DRE up to 195.0 $W.m^{-2}$. As suggested by the approximation given by Lenoble et al. [1982] (Eq. (1)), such large values are obtained for an important amount of absorbing aerosols collocated with a very bright cloud (i.e. high COT value). However, 77% of the pixels have a DRE lower than 60 $W.m^{-2.}$ In contrast, the radiative impact is found to be very weak, even slightly negative, on the south of the scene, where the clouds are the thinnest and the aerosols less absorbing and in small amount. On average over the region, the instantaneous radiative forcing is evaluated at 36.5 $W.m^{-2}$.

4.1.2. Siberian biomass burning aerosols

High northern latitudes are also subject to forest fires from June to October. They are mostly from natural origin following favorable climatic conditions [Stocks et al., 2001] and Siberia is one of the most affected areas by boreal fires [Zhang et al., 2003] leading to significant production of smoke. These aerosols can be transported over long distance [Jaffe et al., 2004] and may result in a non-negligible radiative impact [Lee et al., 2005; Péré et al., 2014]. Wild fires have occurred on the Eastern part of Siberia in July 2008 [Paris et al., 2009]. On 3rd July, aerosols have been detected above clouds (Fig. 6b), over the Sea of Okhotsk. Backward trajectories have shown that they came from the inland of Russia and the MODIS fire product [Giglio et al., 2003] suggests that they may be attributable to fires that took place on the Russian east coast. According to CALIOP, the cloud top is at around 1 km and the aerosol layer is located at about 2 km in the north of the scene (latitude 55°) and goes up to 4 km as we move southward (latitude 45°).

The results of the algorithm are reported in Fig. 8. Like for the previous case, the scene reveals an important amount of particles transported above clouds with an average ACAOT (Fig. 8a) of 0.31 and a peak at 3.0 southward of the Kamchatka Peninsula (latitude 50°). On the northwest side of the peninsula, aerosol radii are found to be between 0.10 and 0.12 µm and, on the other side, the retrieved radii are a bit larger (between 0.12 and 0.16 µm). In parallel, slightly larger values of the angström exponent (Fig. 8b) are found in the upper part of the scene (mean value of 2.19) than southward (mean value of 2.02). Despite the fact that aerosols have the same size as for the African event, the angström exponent reached higher

values for the boreal emission. This is explained by the difference in the aerosol absorption properties. The evaluated SSA (shown Fig. 8c) appears to be closer to 1.0 with a mean value of 0.959 against 0.840 for the previous case study. It points out the scattering nature of the boreal biomass burning aerosols compared to the African savannah ones, in accordance with the study of Dubovik et al. [2002]. Moreover, one can also note the variability of the aerosol absorption of this event: the northern part is associated not only to smallest particles, but also to more absorbing particles with SSA of 0.943 (i.e. a mean complex refractive index of 0.008) compared to 0.964 (respectively 0.005) in the south. This difference may come from aerosol aging: back trajectories suggest that air masses left inland Russia 3 days before arriving to the Southern area while it took only 1 day to arrive in the Northern part of the plume.

Like for the African biomass burning event, the ACCOT (Fig. 8d) is found to be in good spatial agreement with the MODIS product. However, given the weak absorbing character of the overlying aerosol layer, the biases between the two methods (Fig. 8e) are minimal. The thickest clouds are associated with the largest MODIS underestimation (bias up to +12.0). Moreover, one can also note the MODIS overestimation of the COT for thin cloud (bias up to −10.7).

The evaluation of the DRE obtained for this event is presented in Fig. 8f. Large DRE are observed in the northern part of the scene with values around 45 $W.m^{-2}$ between 54 and 57°N. On the opposite, the southwestern part (longitude lower than 160°E) is associated to large negative DRE of about −50 $W.m^{-2}$. As shown in Eq. (1), the sign of the perturbation depends on the balance between the up-scattering and the absorption of the aerosol layer. A warming effect is expected where the aerosols are absorbing and the clouds are bright enough. On the opposite, if the cloud is not optically thick (i.e. COT <10) and the aerosols is scattering (SSA close to 1), the particle layer enhances the albedo of the scene leading to a local cooling. However, these large warming and cooling effects are spatially limited and 88% of the scene have a DRE ranging from −30 to +30 $W.m^{-2}$. On average, the radiative impact is almost neutral with a mean DRE of about −3.5 $W.m^{-2}$.

4.1.3. Saharan dust

The last case study is related to a Saharan dust lifting that has been transported westward over the Atlantic Ocean. These scenes are usually associated with high AOT values. The event of the 4th of August 2008 off the coast of Morocco and Mauritania is not unique. In Fig. 9, we report results for the two POLDER orbits (Fig. 6c). The western part, which is located in the

core of a dust plume, has an average ACAOT (Fig. 9a) of 0.59 at 865 nm. The CALIOP profile gives a cloud top altitude around 2 km and a dust layer at about 4 km. Dust detected off the west coast of Morocco corresponds to a less intense event with a mean ACAOT of 0.27. It has to be remembered that we only retrieve the absorption of dust in the visible (490 nm). Therefore we consider one model of aerosol absorption at 865 nm (i.e. complex part of the refractive index fixed at 0.007), which corresponds to a SSA of 0.984 for this wavelength. Thus, the angström exponent calculated (Fig. 9b) is constant over the scene and is equal to 0.36. Regarding the absorption (Fig. 9c), the two events are again quite distinct. On the one hand, the northern area is associated with SSA at 490 nm around 0.965 with a complex part of the refractive index of 0.001. On the other hand, the western part is slightly more absorbing with a mean SSA at 0.947 and a complex part of the refractive index around 0.002. These values are consistent with those reported by Dubovik et al. [2002].

Here again, the MODIS evaluation of the COT and our estimation (Fig. 9d) are close. Moreover, the fact that dust does not strongly absorb at 865 nm (i.e. the wavelength used for the MODIS retrieval of the COT) explains the small discrepancies observed between the two methods (Fig. 9e) [Haywood et al., 2004]. However, MODIS overestimates the COT for more than 60% of the scene with biases up to −5.3. As for the previous case, this is attributable to the conjunction of thin clouds and scattering aerosols. On average, the bias is equal to −0.2.

Finally, the DRE of the scene has been processed (Fig. 9f). In contrast with the previous cases, the presence of an aerosol layer above clouds results mostly in a cooling effect with a negative DRE over 92% of the scene and an average value of −18.5 $W.m^{-2}$. The maximum and minimum values of the radiative impact (respectively 41.3 and −91.9 $W.m^{-2}$) are reached in the western area. One can also notice the correlation between retrieved ACCOT and the DRE. Since the aerosol properties do not show a lot of variability there, it clearly illustrates the influence of the cloud albedo on the calculation of the radiative impact. Thus, the correct estimation of the COT has to be considered in order to accurately evaluate the radiative impact of ACA.

4.2. Monthly DRE results over the South East Atlantic Ocean

The South East Atlantic Ocean is a preferential area to study aerosol interactions with clouds and radiations because of the aerosol transport above clouds during the August-September dry season. The impact of these biomass burning particles in cloudy scenes are expected to be important not only locally, but also at wider scale through global-teleconnections [Jones et al.,

2009; Jones and Haywood, 2012]. However, the radiative impact of aerosols for the South West African coast remains uncertain for global aerosol models, starting with their direct effect [Myhre et al., 2013a].

The aerosol and cloud properties have been evaluated over the South East Atlantic Ocean during the fire season in August 2006. Important events of biomass burning aerosols over clouds have been detected, especially between the 10^{th} and 24^{th}. The largest events (i.e. with an ACAOT larger than 0.2) represent 28.9 % of the observed scenes. They are characterized by strongly absorbing aerosols with a SSA of 0.867 at 865 nm. Then, the instantaneous radiative forcing of aerosols above clouds has been computed. The monthly averaged DRE values and the corresponding number of observations are reported in Fig. 10a and 10b respectively. Each pixel corresponds to 3 POLDER observations in the mean, with a maximum at 13 observed events off the Angolan coast. As for the case study in August 2008 (Fig. 7), almost all ACA events lead to a warming effect. The maximum values are observed near the coast close to 8°S latitude with averaged DRE around 125 $W.m^{-2}$, which is consistent with the study of De Graaf et al. [2012].

Figure 11 displays the distribution of the DRE values reached during the month. First, it can be noticed that about 14% of the observed scenes have a DRE between 0.0 and 2.5 $W.m^{-2}$. It is important to remember that our method is highly sensitive to the scattering process thanks to polarization measurements. Thus, we are able to well detect scenes with low AOT or with weak absorption. Combined with thick clouds, these events lead to slightly positive DRE values. In contrast, large warming effects have been observed, with DRE greater than 75 $W.m^{-2}$ over 12.7% of the scenes. Less than 0.2% of the pixels are even associated with DRE larger than 220 $W.m^{-2}$. These dramatic values have been obtained for located high loading of absorbing aerosols (i.e. AOT larger than 0.3 and SSA lower than 0.85 at 865 nm) between 9 and 17 August. However, the estimation of the DRE for those intense events has to be considered with caution since our estimation of the aerosol properties may be less accurate. During the first part of the retrieval, we consider that the aerosol absorption does not impact the polarized signal (Fig. 2). This assumption becomes questionable when the amount of aerosols above clouds is very large. On the other hand, around 5% of the events have a negative DRE with a minimum at -41.6 $W.m^{-2}$. The average DRE for August 2006 is 33.5 $W.m^{-2}$, which is of the same order of magnitude than the value obtained by De Graaf et al. [2012] with SCIAMACHY measurements (i.e. 23 $W.m^{-2}$). However, it has to be noted that the two satellite instruments do not observe the scene at the same time. Changes of the scene

between the two measurements [Min et al., 2014] and the difference of solar zenith angles can explain the remaining discrepancies. Furthermore, our algorithm is limited to optically thick cloud (COT > 3) and cannot be applied to fractional cloud coverage.

5. Cloud heterogeneity effects

Our method assumes that clouds are horizontally and vertically homogeneous owing to the use of plan-parallel radiative transfer algorithm (i.e. 1D code). However, lots of studies have shown that the horizontal heterogeneity of clouds affects the scattered radiation measurements through three-dimensional radiative transfer effects [e.g. Marshak and Davis, 2005; Cornet et al., 2013; Zhang et al., 2012]. The cloud heterogeneity may thus affect our estimation of aerosol and cloud properties as well as the DRE. To process the signal considering a more realistic cloud field, a 3D radiative transfer code was used.

5.1. 3D modeling

In order to evaluate the impacts of cloud heterogeneities, the signal (i.e. radiances, polarized radiances and fluxes) for one pixel of an ACA event has been modeled with the Monte-Carlo radiative transfer code 3DMCPOL [Cornet et al., 2010]. The cloud field has been generated using the algorithm 3DCLOUD [Szczap et al., 2014] and the heterogeneity controlled through the inhomogeneity parameter $\rho = \sigma(COT) / COT$, where σ(COT) is the standard deviation of the COT within the pixel. It has to be noted that our algorithm include a filter on the cloud heterogeneity that rejects pixels with σ(COT) larger than 7.0. To process the cloud field, the inhomogeneity parameter ρ has been fixed at 0.6, which represents a standard value for stratocumulus clouds [Szczap et al., 2000a & 2000b]. A statistical analysis of the inhomogeneity parameter has been performed over the ACA scene sampled by the algorithm. It shows that $\rho = 0.6$ can be considered has a high value in this study. The mean COT has been set to 10.0 and the cloud droplet size distribution is assumed to follow a lognormal distribution with $r_{eff} = 11.0$ µm and $v_{eff} = 0.02$. The overlying aerosol layer is composed of fine mode particles with an effective radius of 0.12 µm, an ACAOT of 0.142 at 865 nm and an SSA of 0.781 (i.e. $k = 0.035$). The Radiative Transfer (RT) simulations have been made for a solar incidence angle of 40° at the 3 wavelengths used for the retrievals and for a usual POLDER angular configuration.

5.2. Effects on aerosol and cloud retrieved properties

The estimation of cloud and aerosol properties using our algorithm has been obtained from the 3D modeled signal. As the horizontal heterogeneity of the cloud field influences weakly the polarized signal, which is mostly sensitive to the first orders of scattering, the value of the scattering AOT and the aerosol model retrieved during the first part of the method are not affected.

On the contrary, the total radiances are strongly impacted by the cloud heterogeneity. The total radiances modeled with 3DMCPOL are shown in Fig. 12 as well as the ones modeled with the 1D configuration with the mean cloud properties of the 3D fields. On average, the plan-parallel cloud (i.e. 1D) produces 9.2% at 490 nm and 12.6% at 865 nm more signal than the heterogeneous cloud field. To a lesser extent, the angular behavior is also affected with a more pronounced curve for the 3D modeled signal than for the 1D one. The overestimation due to the 1D assumption influences both wavelengths and consequently the radiance ratio L_{490}/L_{865} is less modified than the total signal. It is 94.1% for the homogeneous cloud and 97.0% for the heterogeneous one. The aerosol SSA, which is principally sensitive to the radiance ratio, is thus not too much impacted by the 3D effects contrary to the retrieved value of the ACCOT. Using a 1D assumption, the aerosol absorption is slightly underestimated with an SSA of 0.794 (k = 0.0325) instead of 0.781 at 865 nm. Therefore, the retrieved AOT is also a little smaller than the expected one (i.e. 0.140 instead of 0.142 at 865 nm). In parallel, our method evaluates the COT at 7.6, which corresponds to an underestimation of 24% comparing to the mean value (i.e. 10.0).

5.3. Effect on the DRE

In the same way that 3D effects influence radiances, fluxes are expected to vary with the heterogeneity of clouds. The quantification of the DRE of aerosols for realistic heterogeneous cloud scene would need 3D radiative transfer modeling of the fluxes, which is too time consuming. To evaluate the error on the DRE due to the homogeneous cloud assumption, we compare the differences between, on the one hand, the 3D TOA fluxes with and without aerosols for the case described in the previous section and, on the other hand, 1D TOA fluxes with the 1D-equivalent aerosol and cloud properties (i.e. COT = 7.6; AOT_{865nm} = 0.140; k = 0.0325). For computing time reason, the analysis focus on fluxes processed at 490 nm. The results obtained from both modeling are shown in Table 2. The fluxes computed with the

1D assumption, which corresponds to the one obtained with our method, is close to the ones given by the 3D modeling (underestimation lower than 2.5%). We can also note that the difference between 3D and 1D modeling is smaller for the polluted cloud scene than for the clean cloud, which means that the aerosols tend to smooth the underneath cloud heterogeneity. The exact $DRE_{0.490\mu m}$ (i.e. computed with the 3D modeling) is equal to 92.06 $W.m^{-2}.\mu m^{-1}$ while we have obtained 81.92 $W.m^{-2}.\mu m^{-1}$ with the 1D assumption. Therefore, considering a plan-parallel cloud for both retrieval and DRE processing leads to slightly underestimate the radiative impact of aerosols, in case of cloud heterogeneity. For the scenes presented in this paper (i.e. which meet our selection criteria), the obtained values can be seen as a lower bound for the ACA DRE. Finally, let us mention that this error is expected to be smaller at higher wavelength and consequently for the solar DRE since the effect of aerosol absorption is the largest in the UV.

6. Conclusion

In this study, we introduced a new approach for the retrieval of aerosol and cloud properties (i.e. AOT, SSA and COT) when an aerosol layer is overlying a liquid cloud above the ocean. Its range of application is restricted to homogeneous clouds with COT larger than 3. The strong point of the algorithm is to combine the sensitivity provided by both total and polarized measurements from the passive satellite instrument POLDER. In a first step, the information on the scattering state of the aerosol layer is given by polarized radiances. The presence of an aerosol layer above a thick liquid cloud leads to a significant enhancement of the polarization at side scattering angle that is used to retrieve the scattering AOT and the aerosol size. Then, these properties together with total radiances are used to determine simultaneously the absorption of the aerosol layer and the COT. In that way, this method allows retrieving the aerosol layer properties with minimum assumptions and the cloud properties corrected from the aerosol absorption.

Nevertheless, the impact of the approximations and the assumptions of the method have been assessed. The largest incertitude about the SSA is due to the approximation about the weak sensitivity of polarized radiances to absorption. When the aerosol size distribution is dominated by the fine mode, an underestimation of −0.055 can be expected for extreme event of absorbing aerosols above clouds (i.e. $AOT_{865nm} = 0.6$ and $SSA_{865nm} = 0.77$). Otherwise, the bias on the SSA is below 0.03. It has to be pointed out that the underestimation of the SSA always goes together with an underestimation of the scattering AOT. As a consequence, the

algorithm presented here provides a reliable estimation of the absorption AOT, which is among the most important parameters to evaluate the DRE of aerosols above clouds.

The algorithm has shown its ability to retrieved aerosol and cloud properties for three case studies with very different characteristics. The first one is related to a biomass burning event off the South West African coast, which is a scene frequently used for ACA studies. As expected, these aerosols are found to be strongly absorbing with SSA of 0.84 at 865 nm. Moreover, the COT given by MODIS is largely underestimated over the scene, which highlights the importance of taking into account the absorption of aerosol for the COT retrieval. The second example is devoted to Siberian biomass burning. It illustrates the high variability of ACA properties with an average particle SSA at 0.96. In contrast with the previous scene, the enhancement of scattering due to these aerosols may cause an overestimation of the COT by MODIS. Finally, the algorithm can be used not only on fine mode aerosols above clouds, but also on dust particles. The study of Saharan dust transported over clouds has revealed the ability of the method to evaluate the differential dust absorption of visible light at short wavelength for a given value at 865 nm. It should be added that low differences have been observed between our COT retrieval and the MODIS one where the AOT is the smallest. Such biases have already been observed by Zeng et al. [2012] and are primarily due to the difference of instrument characteristics.

Furthermore, we developed a procedure to evaluate the DRE of aerosols above clouds based on exact calculations. The radiative impact processed for the three case studies confirms the need of accurately quantifying the aerosol absorption and the brightness of the underneath cloud. Thick clouds in association with highly absorbing aerosols translate into a warming effect and can reach high DRE values as for the African biomass burning aerosols. On the opposite, a cooling effect can be observed for scenes with low aerosol absorption and thin clouds as for the Saharan dust event. The estimated DRE for Siberian biomass burning aerosols is spatially contrasting since both cloud and aerosol properties show variability.

The algorithm has been applied to one month of measurements over the South East Atlantic Ocean. August 2006 is characterized by important amount of absorbing biomass burning aerosols above the permanent stratocumulus deck. The DRE has been processed. The presence of the aerosol layer above bright clouds is responsible for a large radiative impact. The monthly averaged value over the scene is estimated at 33.5 $W.m^{-2}$, which is of the same order of magnitude as the estimation of De Graaf et al. [2012] (i.e. 23 $W.m^{-2}$). Let us point out that differences between the result of this study and the literature are expected and are mainly

due to the selection of the AAC scenes: this analysis does not include thin clouds (i.e. COT < 3) and scene with fractional cloud coverage which leads to biased high the DRE. The algorithm developed here could provide aerosol and cloud properties that can be used to better constrain numerical models, leading to a reduction of their uncertainty.

Some efforts still have to be done to enhance our knowledge on aerosols above clouds. Currently, the described method allows the retrieval of aerosol and cloud properties only over the ocean. The procedure has to be extended to ACA events over land, which requires paying attention to the contribution of the surface to the measurements. Another key point is the study of aerosols over thin layer of clouds. The first part of the algorithm relies on the independence of the polarized signal for optically thick clouds. To go further, scenes with aerosols in fractional cloud coverage have to be investigated. The cloud inhomogeneity also affects the radiances and fluxes of ACA scenes. Thus, we have examined the impact of considering a plan-parallel cloud on the aerosol and cloud properties as well as the DRE. On the one hand, the retrieval of aerosol properties is weakly biased since polarized radiances and radiance ratio are not significantly affected by cloud heterogeneity. Finally, the homogeneous cloud assumption leads to an underestimation of the DRE of aerosols. This bias remains small in this study because scenes with too heterogeneous clouds are rejected. However, a thorough analysis of the effect of the homogeneous cloud assumption on the estimation of the DRE would provide a significant contribution to the scientific field.

The first results obtained for ACA scenes over the ocean are promising and confirms the need of both global and temporal distribution aerosol and cloud properties. Thus, our next target will be to analyze POLDER measurements over the whole database and to give a first estimation of the global DRE of aerosols over cloudy skies.

Acknowledgements

This work has been supported by the Programme National de Télédétection Spatiale (PNTS, http://www.insu.cnrs.fr/pnts), grant n° PNTS-2013-10 and n° PNTS-2014-02. The authors are grateful to CNES, NASA, and the ICARE data and services center.

The authors acknowledge the support of France Grilles for providing computing resources on the French National Grid Infrastructure.

1 The authors would like to thank the reviewers for their valuable comments and suggestions
2 that considerably improved the article. Finally, they are grateful to the editor, Paola Formenti,
3 for her help during the editorial process.
4

References

Ackerman, A. S., Toon, O. B., Stevens, D. E., Heymsfield, A. J., Ramanathan, V., & Welton, E. J. (2000). Reduction of tropical cloudiness by soot. *Science*, *288*(5468), 1042-1047.

Albrecht, B. A. (1989). Aerosols, cloud microphysics, and fractional cloudiness. *Science*, *245*(4923), 1227-1230.

Balkanski, Y., Schulz, M., Claquin, T., & Guibert, S. (2007). Reevaluation of Mineral aerosol radiative forcings suggests a better agreement with satellite and AERONET data. *Atmospheric Chemistry and Physics*, *7*(1), 81-95.

Bréon, F. M., Tanré, D., & Generoso, S. (2002). Aerosol effect on cloud droplet size monitored from satellite. *Science*, *295*(5556), 834-838.

Chakrabarty, R. K., Moosmüller, H., Chen, L. W., Lewis, K., Arnott, W. P., Mazzoleni, C., Dubey, M. K., Wold, C. E., Hao, W. M., & Kreidenweis, S. M. (2010). Brown carbon in tar balls from smoldering biomass combustion. *Atmospheric Chemistry and Physics*, *10*(13), 6363-6370.

Chand, D., Anderson, T. L., Wood, R., Charlson, R. J., Hu, Y., Liu, Z., & Vaughan, M. (2008). Quantifying above-cloud aerosol using spaceborne lidar for improved understanding of cloudy-sky direct climate forcing. *Journal of Geophysical Research: Atmospheres (1984–2012)*, *113, D13206, doi: 10.1029/2007JD009433*.

Chand, D., Wood, R., Anderson, T. L., Satheesh, S. K., & Charlson, R. J. (2009). Satellite-derived direct radiative effect of aerosols dependent on cloud cover. *Nature Geoscience*, *2*(3), 181-184.

Coddington, O. M., Pilewskie, P., Redemann, J., Platnick, S., Russell, P. B., Schmidt, K. S., & Vukicevic, T. (2010). Examining the impact of overlying aerosols on the retrieval of cloud optical properties from passive remote sensing. *Journal of Geophysical Research: Atmospheres (1984–2012)*, *115, D10211, doi: 10.1029/2009JD012829*.

Cole, A. E., Court, A., & Kantor, A.J. (1965). Model atmospheres. *Handbook of geophysics and space environment,* in: Chap. 2, edited by: Valley, S. L., McGraw-Hill, New York, 1965.

Cornet, C., Labonnote, L. C. and Szczap, F. (2010). Three-dimensional polarized Monte Carlo atmospheric radiative transfer model (3DMCPOL): 3D effects on polarized

visible reflectances of a cirrus cloud. *Journal of Quantitative Spectroscopy and Radiative Transfer*, *111*(1), 174-186.

Cornet, C., Szczap, F., Labonnote, L. C., Fauchez, T., Parol, F., Thieuleux, F., Riedi, J., Dubuisson, P., & Ferlay, N. (2013). Evaluation of cloud heterogeneity effects on total and polarized visible radiances as measured by POLDER/PARASOL and consequences for retrieved cloud properties. In *RADIATION PROCESSES IN THE ATMOSPHERE AND OCEAN (IRS2012): Proceedings of the International Radiation Symposium (IRC/IAMAS)* (Vol. 1531, No. 1, pp. 99-102). AIP Publishing.

Costantino, L., & Bréon, F. M. (2013). Satellite-based estimate of aerosol direct radiative effect over the South-East Atlantic. *Atmospheric Chemistry and Physics Discussions*, *13*(9), 23295-23324.

Cox, C., & Munk, W. (1954). Measurement of the roughness of the sea surface from photographs of the sun's glitter. *JOSA*, *44*(11), 838-850.

De Graaf, M., Tilstra, L. G., Wang, P., & Stammes, P. (2012). Retrieval of the aerosol direct radiative effect over clouds from spaceborne spectrometry. *Journal of Geophysical Research: Atmospheres (1984–2012)*, *117*, D07207, doi:10.1029/2011JD017160.

De Haan, J. F., Bosma, P. B., & Hovenier, J. W. (1987). The adding method for multiple scattering calculations of polarized light. *Astronomy and Astrophysics*, *183*, 371-391.

Deuzé, J. L., Herman, M., & Santer, R. (1989). Fourier series expansion of the transfer equation in the atmosphere-ocean system. *Journal of Quantitative Spectroscopy and Radiative Transfer*, *41*(6), 483-494.

Dubuisson P., J.-C. Roger, M. Mallet, O. Dubovik, a code to compute the direct solar radiative forcing: application to anthropogenic aerosols during the Escompte experiment, Proceedings of IRS 2004: Current Problems in Atmospheric Radiation, 23–28 August 2004, Busan, Korea, 2004.

Dubovik, O., Holben, B., Eck, T. F., Smirnov, A., Kaufman, Y. J., King, M. D., Tanré, D., & Slutsker, I. (2002). Variability of absorption and optical properties of key aerosol types observed in worldwide locations. *Journal of the Atmospheric Sciences*, *59*, 590–608, doi:10.1175/1520- 0469(2002)059<0590:VOAAOP>2.0.CO;2, 2002.

Fougnie, B., Bracco, G., Lafrance, B., Ruffel, C., Hagolle, O., & Tinel, C. (2007). PARASOL in-flight calibration and performance. *Applied optics*, *46*(22), 5435-5451.

Giglio, L., Descloitres, J., Justice, C. O., & Kaufman, Y. J. (2003). An enhanced contextual fire detection algorithm for MODIS. *Remote sensing of environment*, *87*(2), 273-282.

Hasekamp, O. P.: Capability of multi-viewing-angle photo-polarimetric measurements for the simultaneous retrieval of aerosol and cloud properties, *Atmospheric Measurement Techniques.*, 3, 839–851, doi:10.5194/amt-3-839-2010, 2010.

Haywood, J. M., Osborne, S. R., & Abel, S. J. (2004). The effect of overlying absorbing aerosol layers on remote sensing retrievals of cloud effective radius and cloud optical depth. *Quarterly Journal of the Royal Meteorological Society*, *130*(598), 779-800.

Herman, M., Deuzé, J. L., Marchand, A., Roger, B., & Lallart, P. (2005). Aerosol remote sensing from POLDER/ADEOS over the ocean: Improved retrieval using a nonspherical particle model. *Journal of Geophysical Research: Atmospheres (1984–2012)*, *110*, D10S02, doi:10.1029/2004JD004798.

Hu, Y., Vaughan, M., Liu, Z., Powell, K., & Rodier, S. (2007). Retrieving optical depths and lidar ratios for transparent layers above opaque water clouds from CALIPSO lidar measurements. *Geoscience and Remote Sensing Letters, IEEE*, *4*(4), 523-526.

Jaffe, D., Bertschi, I., Jaeglé, L., Novelli, P., Reid, J. S., Tanimoto, H., Vingarzan, R., & Westphal, D. L. (2004). Long-range transport of Siberian biomass burning emissions and impact on surface ozone in western North America. *Geophysical Research Letters*, *31*, L16106, doi:10.1029/2004GL020093.

Jethva, H., Torres, O., Remer, L. A., & Bhartia, P. K. (2013). A color ratio method for simultaneous retrieval of aerosol and cloud optical thickness of above-cloud absorbing aerosols from passive sensors: Application to MODIS measurements, IEEE T. Geosci. Remote Sens, 51, 3862–3870, 2013.

Jethva, H., Torres, O., Waquet, F., Chand, D., & Hu, Y. (2014). How do A-train sensors intercompare in the retrieval of above-cloud aerosol optical depth? A case study-based assessment. *Geophysical Research Letters,* 41, 186–192, doi:10.1002/2013GL058405, 2014.

Johnson, B. T., Shine, K. P., & Forster, P. M. (2004). The semi-direct aerosol effect: Impact of absorbing aerosols on marine stratocumulus. *Quarterly Journal of the Royal Meteorological Society*, *130*(599), 1407-1422.

Johnson, B. T., Osborne, S. R., Haywood, J. M., & Harrison, M. A. J. (2008). Aircraft measurements of biomass burning aerosol over West Africa during DABEX. *Journal of Geophysical Research: Atmospheres (1984–2012)*,*113*(D23).

Jones, A., Haywood, J., & Boucher, O. (2009). Climate impacts of geoengineering marine stratocumulus clouds. *Journal of Geophysical Research: Atmospheres (1984–2012)*, *114*, D10106, doi:10.1029/2008JD011450.

Jones, A., & Haywood, J. M. (2012). Sea-spray geoengineering in the HadGEM2-ES earth-system model: radiative impact and climate response. *Atmospheric Chemistry and Physics*, *12*(22), 10887-10898.

Kaufman, Y. J., Koren, I., Remer, L. A., Rosenfeld, D., & Rudich, Y. (2005). The effect of smoke, dust, and pollution aerosol on shallow cloud development over the Atlantic Ocean. *Proceedings of the National Academy of Sciences of the United States of America*, *102*(32), 11207-11212.

Kirchstetter, T. W., Novakov, T., & Hobbs, P. V. (2004). Evidence that the spectral dependence of light absorption by aerosols is affected by organic carbon. *Journal of Geophysical Research: Atmospheres (1984–2012)*, *109*, D21208, doi:10.1029/ 2004JD004999.

Knobelspiesse, K., Cairns, B., Redemann, J., Bergstrom, R. W., & Stohl, A. (2011). Simultaneous retrieval of aerosol and cloud properties during the MILAGRO field campaign. *Atmospheric Chemistry and Physics*, *11*(13), 6245-6263.

Koren, I., Kaufman, Y. J., Remer, L. A., & Martins, J. V. (2004). Measurement of the effect of Amazon smoke on inhibition of cloud formation. *Science*, *303*(5662), 1342-1345.

Leahy, L. V., Anderson, T. L., Eck, T. F., & Bergstrom, R. W. (2007). A synthesis of single scattering albedo of biomass burning aerosol over southern Africa during SAFARI 2000. *Geophysical Research Letters*, *34*, L12814, doi:10.1029/2007GL029697.

Lee, K. H., Kim, J. E., Kim, Y. J., Kim, J., & von Hoyningen-Huene, W. (2005). Impact of the smoke aerosol from Russian forest fires on the atmospheric environment over Korea during May 2003. *Atmospheric Environment*, *39*(1), 85-99.

Lenoble, J., Tanré, D., Deschamps, P. Y., & Herman, M. (1982). A simple method to compute the change in earth-atmosphere radiative balance due to a stratospheric aerosol layer. *Journal of the Atmospheric Sciences*, *39*(11), 2565-2576.

Marshak, A., & Davis, A. (Eds.). (2005). *3D Radiative Transfer in Cloudy Atmospheres* (Vol. 5117). Springer, Berlin, Heidelberg, 2005.

Meyer, K., Platnick, S., Oreopoulos, L., & Lee, D. (2013). Estimating the direct radiative effect of absorbing aerosols overlying marine boundary layer clouds in the southeast Atlantic using MODIS and CALIOP. *Journal of Geophysical Research: Atmospheres*, *118*(10), 4801-4815.

Min, M., & Zhang, Z. (2014). On the influence of cloud fraction diurnal cycle and sub-grid cloud optical thickness variability on all-sky direct aerosol radiative forcing. *Journal of Quantitative Spectroscopy and Radiative Transfer*, *142*, 25-36.

Myhre, G., Samset, B. H., Schulz, M., Balkanski, Y., Bauer, S., Berntsen, T. K., Bian, H., Bellouin, N., Chin, M., Diehl, T., Easter, R. C., Feichter, J., Ghan, S. J., Hauglustaine, D., Iversen, T., Kinne, S., Kirkevåg, A., Lamarque, J.-F., Lin, G., Liu, X., Lund, M. T., Luo, G., Ma, X., van Noije, T., Penner, J. E., Rasch, P. J., Ruiz, A., Seland, Ø., Skeie, R. B., Stier, P., Takemura, T., Tsigaridis, K., Wang, P., Xu, L., Yu, H., Yoon, J.-F., Zhang, H., & Zhou, C. (2013a). Radiative forcing of the direct aerosol effect from AeroCom Phase II simulations. *Atmospheric Chemistry & Physics*, *13*(4).

Myhre, G., D. Shindell, F.-M. Bréon, W. Collins, J. Fuglestvedt, J. Huang, D. Koch, J.-F. Lamarque, D. Lee, B. Mendoza, T. Nakajima, A. Robock, G. Stephens, T. Takemura and H. Zhang, 2013: Anthropogenic and Natural Radiative Forcing. In: Climate Change 2013: The Physical Science Basis. Contribution of Working Group I to the Fifth Assessment Report of the Intergovernmental Panel on Climate Change, edited by: Stocker, T.F., D. Qin, G.-K. Plattner, M. Tignor, S.K. Allen, J. Boschung, A. Nauels, Y. Xia, V. Bex and P.M. Midgley, Cambridge University Press, Cambridge, UK and New York, NY, USA, 571-657, 2013b

Nakajima, T., & King, M. D. (1990). Determination of the optical thickness and effective particle radius of clouds from reflected solar radiation measurements. Part I: Theory. *Journal of the atmospheric sciences*, *47*(15), 1878-1893.

Paris, J. D., Stohl, A., Nédélec, P., Arshinov, M. Y., Panchenko, M. V., Shmargunov, V. P., Law, K. S., Belan, B. D., & Ciais, P. (2009). Wildfire smoke in the Siberian Arctic in summer: source characterization and plume evolution from airborne measurements. *Atmospheric Chemistry and Physics*, *9*(23), 9315-9327.

Péré, J. C., Bessagnet, B., Mallet, M., Waquet, F., Chiapello, I., Minvielle, F., Pont, V., & Menut, L. (2014). Direct radiative effect of the Russian wildfires and its impact on air temperature and atmospheric dynamics during August 2010. *Atmospheric Chemistry and Physics*, *14*(4), 1999-2013.

Peters, K., Quaas, J., & Bellouin, N. (2011). Effects of absorbing aerosols in cloudy skies: a satellite study over the Atlantic Ocean. *Atmospheric Chemistry and Physics*, *11*(4), 1393-1404.

Ramanathan, V., Crutzen, P. J., Kiehl J. T., & Rosenfeld D. (2001). Aerosols, climate, and the hydrological cycle. *Science*, *294*(5549), 2119-2124.

Rossow, W. B., Garder, L. C., & Lacis, A. A. (1989). Global, seasonal cloud variations from satellite radiance measurements. Part I: Sensitivity of analysis. *Journal of Climate*, *2*(5), 419-458.

Sayer, A. M., Hsu, N. C., Eck, T. F., Smirnov, A., & Holben, B. N. (2014). AERONET-based models of smoke-dominated aerosol near source regions and transported over oceans, and implications for satellite retrievals of aerosol optical depth. *Atmospheric Chemistry and Physics*, *14*(20), 11493-11523.

Stocks, B. J., Wotton, B. M., Flannigan, M. D., Fosberg, M. A., Cahoon, D. R., & Goldammer, J. G. (2001). Boreal forest fire regimes and climate change. *Remote Sensing and Climate Modeling: Synergies and Limitations* (pp. 233-246). Springer Netherlands.

Szczap, F., Isaka, H., Saute, M., Guillemet, B., & Gour, Y. (2000a). Inhomogeneity effects of 1D and 2D bounded cascade model clouds on their effective radiative properties. *Physics and Chemistry of the Earth, Part B: Hydrology, Oceans and Atmosphere*, *25*(2), 83-89.

Szczap, F., Isaka, H., Saute, M., Guillemet, B., & Ioltukhovski, A. (2000b). Effective radiative properties of bounded cascade nonabsorbing clouds: Definition of the equivalent homogeneous cloud approximation. *Journal of Geophysical Research: Atmospheres (1984–2012)*, *105*(D16), 20617-20633.

Szczap, F., Gour, Y., Fauchez, T., Cornet, C., Faure, T., Jourdan, O., Penide, G., and Dubuisson, P.: A flexible three-dimensional stratocumulus, cumulus and cirrus cloud generator (3DCLOUD) based on drastically simplified atmospheric equations and the Fourier

transform framework, *Geoscience Model Development*, 7, 1779–1801, doi:10.5194/gmd-7-1779-2014, 2014.

Tanré, D., Bréon, F. M., Deuzé, J. L., Dubovik, O., Ducos, F., François, P., Goloub, P., Herman, M., Lifermann, A., & Waquet, F. (2011). Remote sensing of aerosols by using polarized, directional and spectral measurements within the A-Train: the PARASOL mission. *Atmospheric Measurement Techniques*, *4*(7), 1383-1395.

Torres, O., Jethva, H., & Bhartia, P. K. (2012). Retrieval of Aerosol Optical Depth above Clouds from OMI Observations: Sensitivity Analysis and Case Studies. *Journal of the Atmospheric Sciences*, *69*, 1037–1053, doi: 10.1175/JAS-D-11-0130.1.

Twomey, S. (1974). Pollution and the planetary albedo. *Atmospheric Environment (1967)*, *8*(12), 1251-1256.

Twomey, S. (1977). The influence of pollution on the shortwave albedo of clouds. *Journal of the Atmospheric Sciences*, *34*(7), 1149-1152.

Vanbauce, C., Cadet, B., & Marchand, R. T. (2003). Comparison of POLDER apparent and corrected oxygen pressure to ARM/MMCR cloud boundary pressures. *Geophysical Research Letters*, *30*, 1212, doi:10.1029/2002GL016449.

Waquet, F., Riedi, J., Labonnote, L. C., Goloub, P., Cairns, B., Deuzé, J. L., & Tanré, D. (2009). Aerosol Remote Sensing over Clouds Using A-Train Observations. *Journal of the Atmospheric Sciences*, *66*, 2468–2480, doi: 10.1175/2009JAS3026.1.

Waquet, F., Cornet, C., Deuzé, J. L., Dubovik, O., Ducos, F., Goloub, P., Herman, M., Lapyonok, T., Labonnote, L., C., & Vanbauce, C. (2013a). Retrieval of aerosol microphysical and optical properties above liquid clouds from POLDER/PARASOL polarization measurements. *Atmospheric Measurement Techniques*, *6*(4), 991-1016.

Waquet, F., Peers, F., Ducos, F., Goloub, P., Platnick, S., Riedi, J., Tanré, D., & Thieuleux, F. (2013b). Global analysis of aerosol properties above clouds. *Geophysical Research Letters*, *40*(21), 5809-5814.

Wilcox, E. M., & Platnick, S. (2009). Estimate of the impact of absorbing aerosol over cloud on the MODIS retrievals of cloud optical thickness and effective radius using two independent retrievals of liquid water path. *Journal of Geophysical Research: Atmospheres (1984–2012)*, *114*, D05210, doi:10.1029/2008JD010589.

Winker, D. M., Vaughan, M. A., Omar, A., Hu, Y., Powell, K. A., Liu, Z., Hunt., W., & Young, S. A. (2009). Overview of the CALIPSO mission and CALIOP data processing

algorithms. *Journal of Atmospheric & Oceanic Technology*, *26*, 2310–2323, doi: 10.1175/2009JTECHA1281.1.

Winker, D. M., Tackett, J. L., Getzewich, B. J., Liu, Z., Vaughan, M. A., & Rogers, R. R. (2013). The global 3-D distribution of tropospheric aerosols as characterized by CALIOP. *Atmospheric Chemistry and Physics*, *13*(6), 3345-3361.

Young, S. A., & Vaughan, M. A. (2009). The retrieval of profiles of particulate extinction from Cloud-Aerosol Lidar Infrared Pathfinder Satellite Observations (CALIPSO) data: Algorithm description. *Journal of Atmospheric & Oceanic Technology*, *26*, 1105–1119, doi: 10.1175/2008JTECHA1221.1.

Zeng, S., Cornet, C., Parol, F., Riedi, J., & Thieuleux, F. (2012). A better understanding of cloud optical thickness derived from the passive sensors MODIS/AQUA and POLDER/PARASOL in the A-Train constellation. *Atmospheric Chemistry and Physics*, *12*(23), 11245-11259.

Zhang, Y. H., Wooster, M. J., Tutubalina, O., & Perry, G. L. W. (2003). Monthly burned area and forest fire carbon emission estimates for the Russian Federation from SPOT VGT. *Remote Sensing of Environment*, *87*(1), 1-15.

	Polarized LUT	Total radiance LUT
Aerosols models		
Vertical distribution	gaussian layer with a mean altitude of 3 km	homogeneous layer between 2 and 3 km
Fine mode:		
Size distribution	lognormal distribution with $\sigma_f = 0.4$ $r_{eff} = 0.06$ to 0.16 µm (by 0.02 µm step)	
Refractive index	1.47 – i.0.01	1.47 – i.k with k = 0.00 to 0.05 (by 0.0025 step)
Dust:		
Size distribution	bimodal lognormal distribution with $\sigma_f = 0.4$ $r_{eff,fine} = 0.35$ µm $r_{eff,coarse} = 2.55$ µm	
Refractive index	1.47 – i.0.0007	1.47 – i.k $k_{865nm} = 0.0007$ $k_{490nm} = 0.0$ to 0.004 (by 0.0005 step)
Cloud models		
Vertical distribution	homogeneous layer from 0 to 0.75 km	homogeneous layer from 0 to 1 km
Size distribution	gamma law with veff = 0.06	
	$r_{eff} = 5$ to 26 µm (by 1 µm step)	$r_{eff} = 10$ µm
Refractive index	$m_{r,490nm} = 1.338$ $m_{r,670nm} = 1.331$ $m_{r,865nm} = 1.330$	

Table 1. Aerosol and cloud model properties used to compute the polarized and total radiance LUT of the POLDER algorithm.

	3D modeling	1D modeling	$(F_{1D}-F_{3D})/F_{3D}$ (%)
$\mathbf{F\uparrow_{cloud+aer}}$	569.01	564.48	-0.79
$\mathbf{F\uparrow_{cloud}}$	661.07	646.40	-2.22
$\mathbf{DRE = F\uparrow_{cloud} - F\uparrow_{cloud+aer}}$	92.06	81.92	-11.01

Table 2. Fluxes for polluted and clean scene and DRE ($W.m^{-2}.\mu m^{-1}$) at the TOA at 0.490 µm modeled using a 3D and 1D assumption.

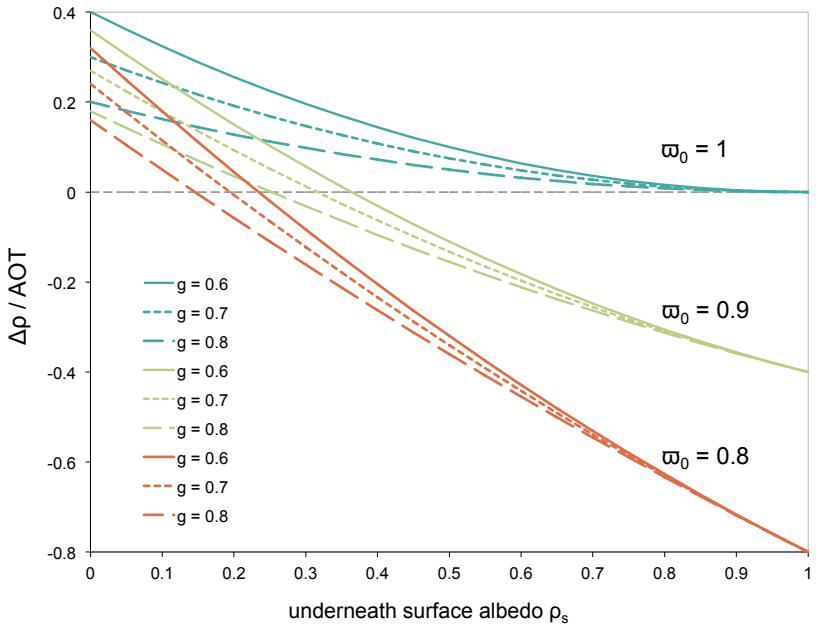

Figure 1. Modification of the albedo of a scene Δρ caused by the presence of an aerosol layer versus the albedo of the underneath surface ρ_s calculated with the approximate expression given by Lenoble et al. [1982]. Dark green lines correspond to purely scattering only aerosols ($\varpi_0 = 1$), light green to aerosols moderately absorbing ($\varpi_0 = 0.9$) and orange lines are for absorbing aerosols ($\varpi_0 = 0.8$) and g is the asymmetry factor.

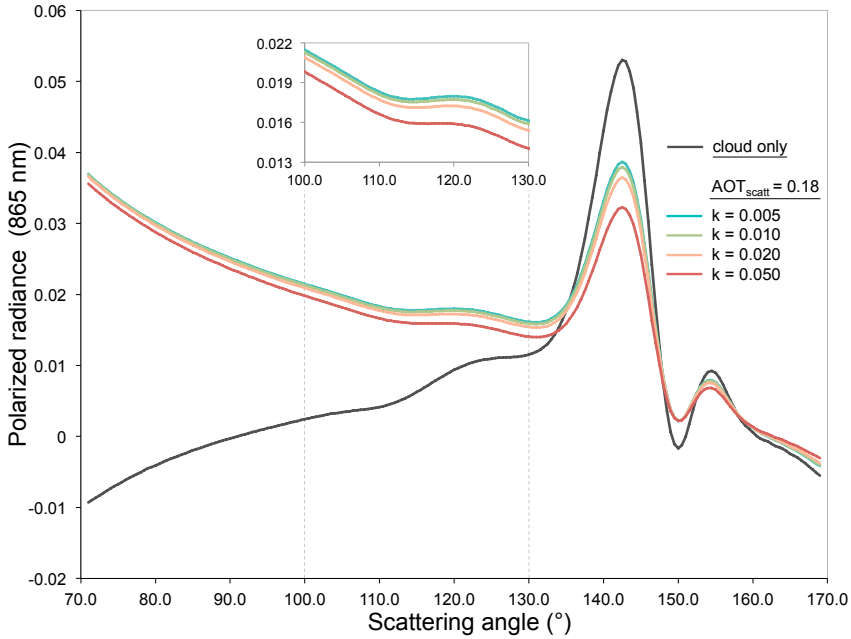

Figure 2. Simulated polarized radiance at 865 nm plotted against the scattering angle. Black line corresponds to the cloud only (COT = 10, r_{eff} = 10 µm). Colored lines are for an aerosol layer above clouds. The effective radius of aerosols is 0.10 µm. Several absorption AOT (i.e. various k) have been considered but the scattering AOT is fixed at 0.18. The inset focuses on polarized radiances of aerosols above clouds for scattering angles between 100° and 130°. Complementary information about vertical distributions and properties of aerosols and clouds can be found in Table 1 (cf. polarized LUT).

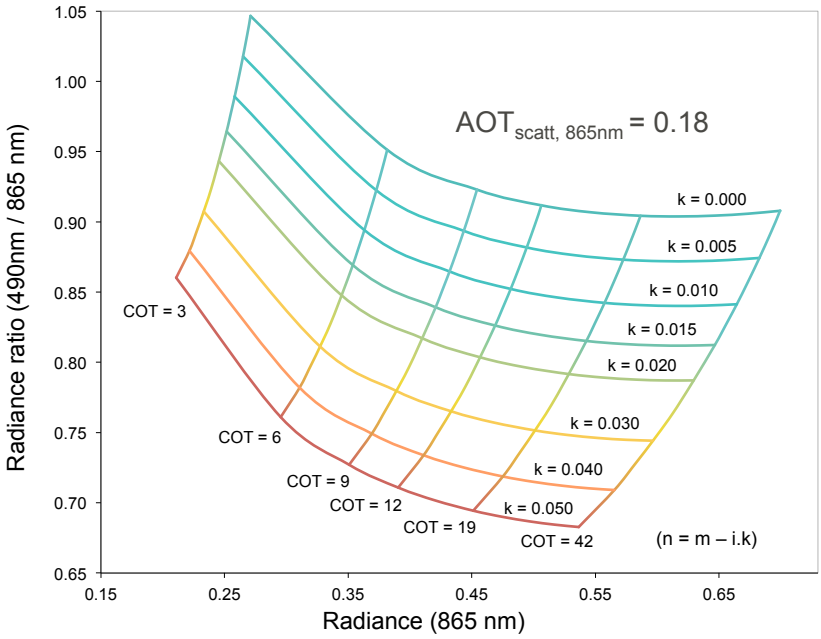

Figure 3. Radiance ratio L_{490nm}/L_{865nm} as a function of the radiance at 865 nm. Signals have been simulated for aerosols with an effective radius of 0.10 µm, an effective radius of cloud droplet of 10 µm (for more information about aerosol and cloud properties and vertical distribution, cf. Table 1, total radiance LUT column). The scattering AOT is set and several absorption AOT as well as several COT are considered. Calculations have been carried out for a solar zenith angle $\theta_s = 41.3°$, a viewing angle $\theta_v = 41.3°$ and a relative azimuth $\varphi_r = 180°$.

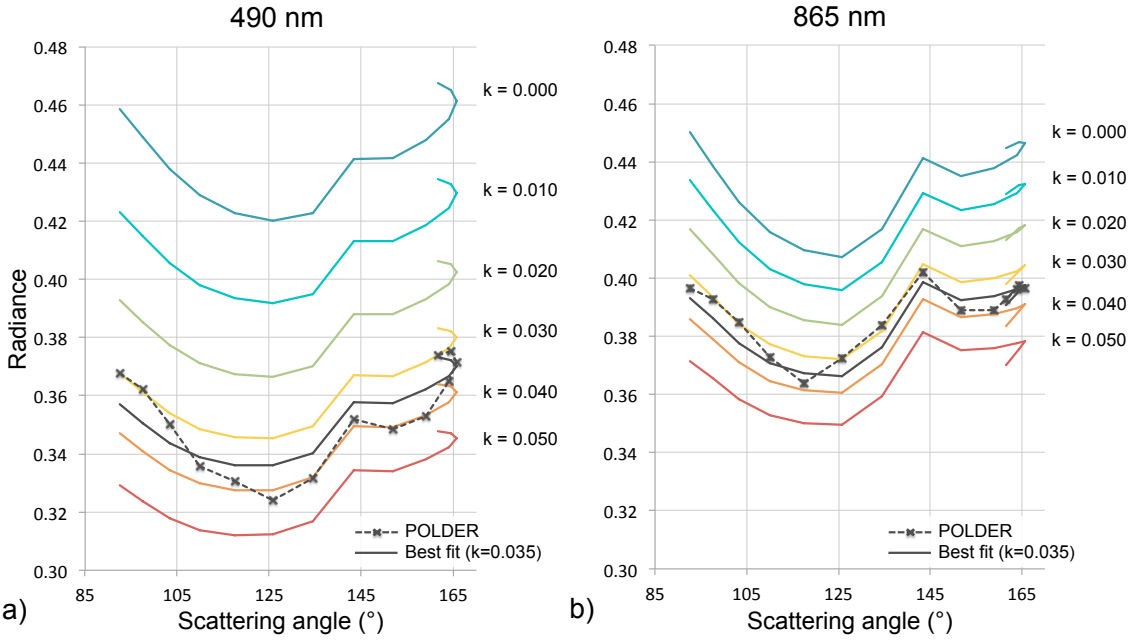

Figure 4. Example of measured and simulated total radiances for one pixel at 490 nm (a) and 865 nm (b). The dashed black lines are for the measurements and the continuous black ones are for the simulated signals corresponding to the solution (i.e. COT = 12.4; k = 0.035; AOT = 0.14). Other colored lines correspond to the signal simulated for the same COT, the same scattering AOT and for several k (i.e. different absorption AOT).

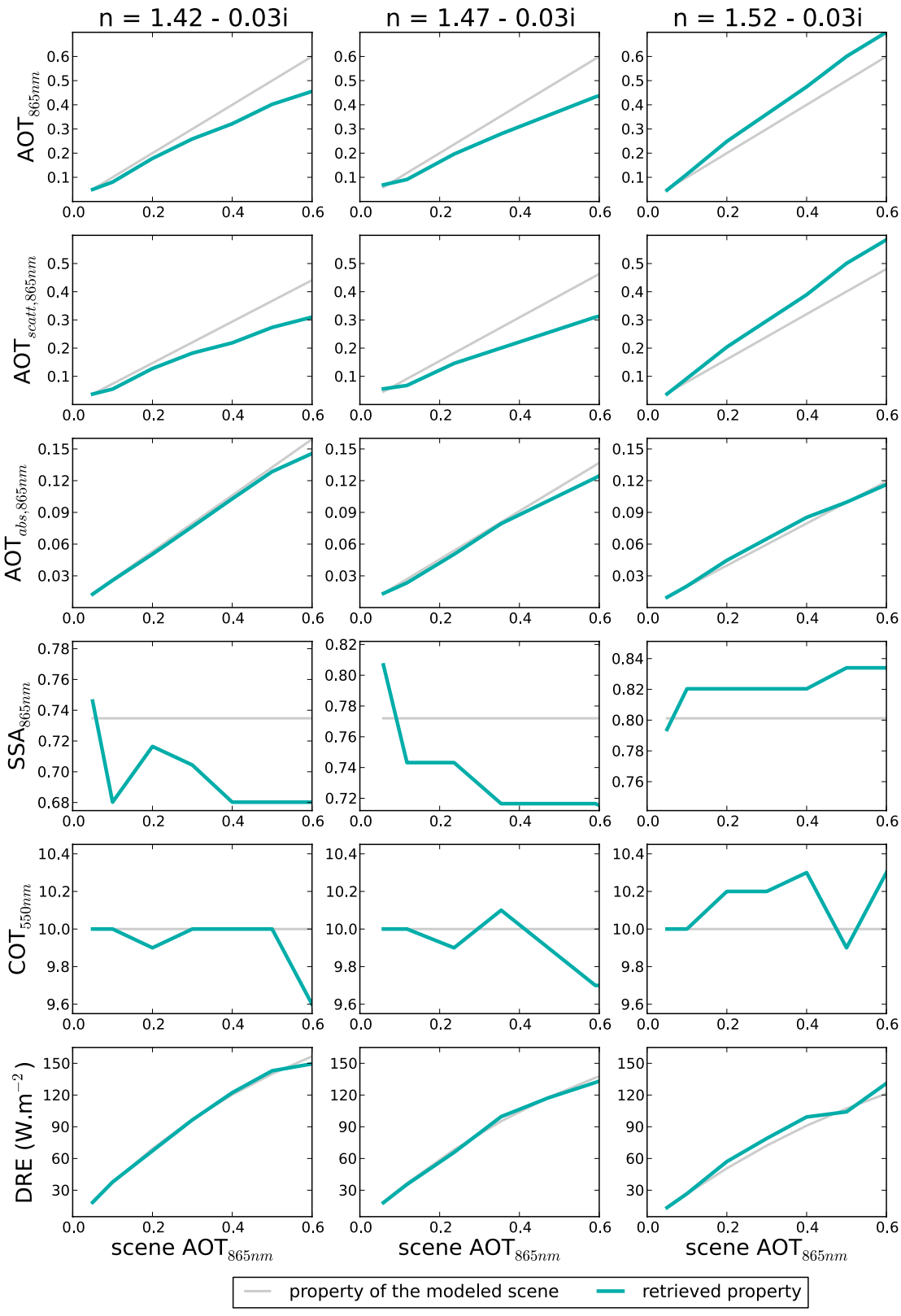

Figure 5. Sensitivity of the properties of an AAC scene with different aerosol models. From top to the bottom: total AOT, scattering AOT, absorption AOT and SSA at 865 nm, COT at 550 nm and the short wave DRE of aerosols. Grey lines correspond to the properties of the actual modeled scene and green lines to those retrieved by the algorithm. The aerosol model of the first column has a refractive index n equal to $1.42 - 0.03i$, the second, $n = 1.47 - 0.03i$ and the third, $n = 1.52 - 0.03i$. Aerosols have an effective radius of 0.1 µm and the effective radius of the cloud water droplets is 10 µm.

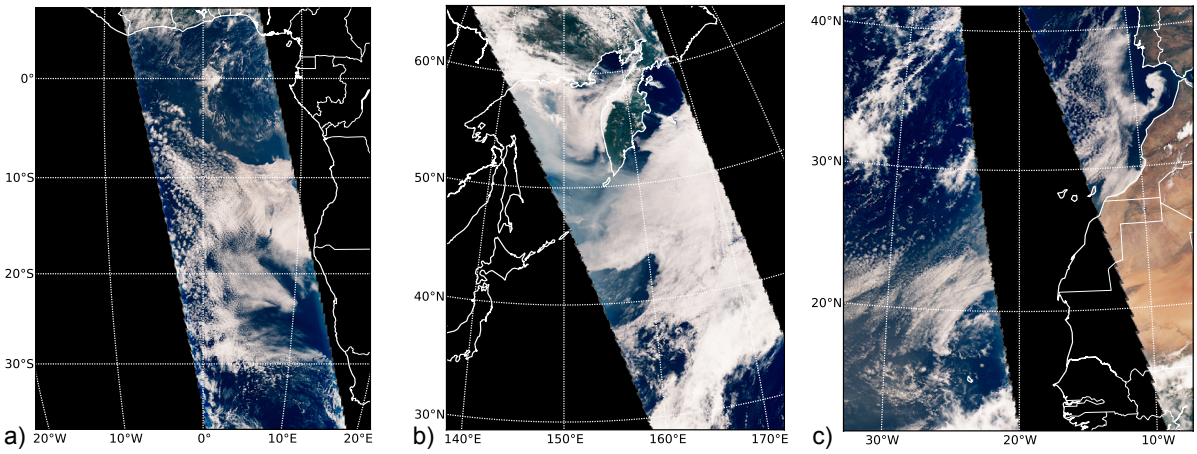

Figure 6. True color POLDER/PARASOL RGB composite (a) over the South East Atlantic Ocean the 4th of August 2008, (b) off the East Russian coast the 3rd of July 2008 and (c) over the North Atlantic Ocean the 4th of August 2008.

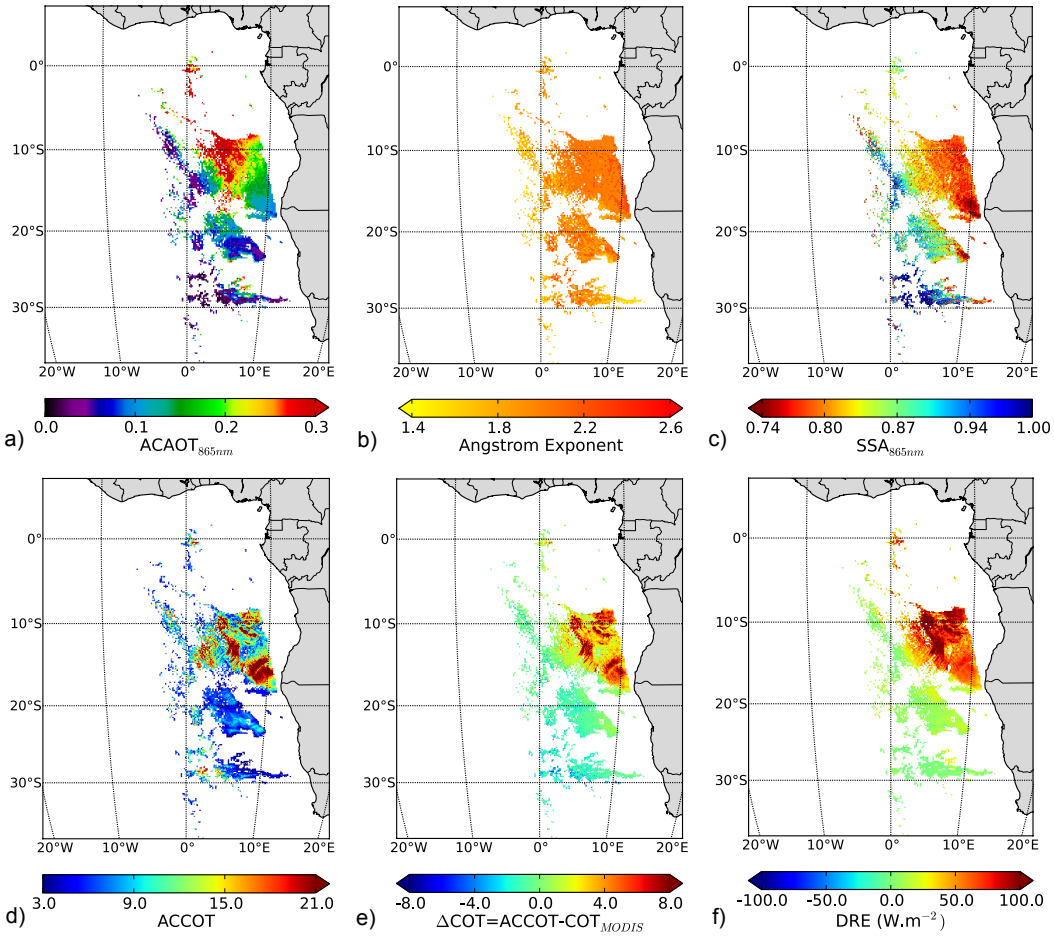

Figure 7. Biomass burning aerosols above clouds off the South West African Coast on 4th August 2008. The panel displays the Above Cloud AOT at 865 nm (a), the Angström Exponent (b), the aerosol SSA at 865 nm (c), the Aerosol Corrected COT at 550 nm (d), the difference ΔCOT of the AACOT and the MODIS COT (e) and the Direct Radiative Effect of aerosols above clouds in W.m-2 (f).

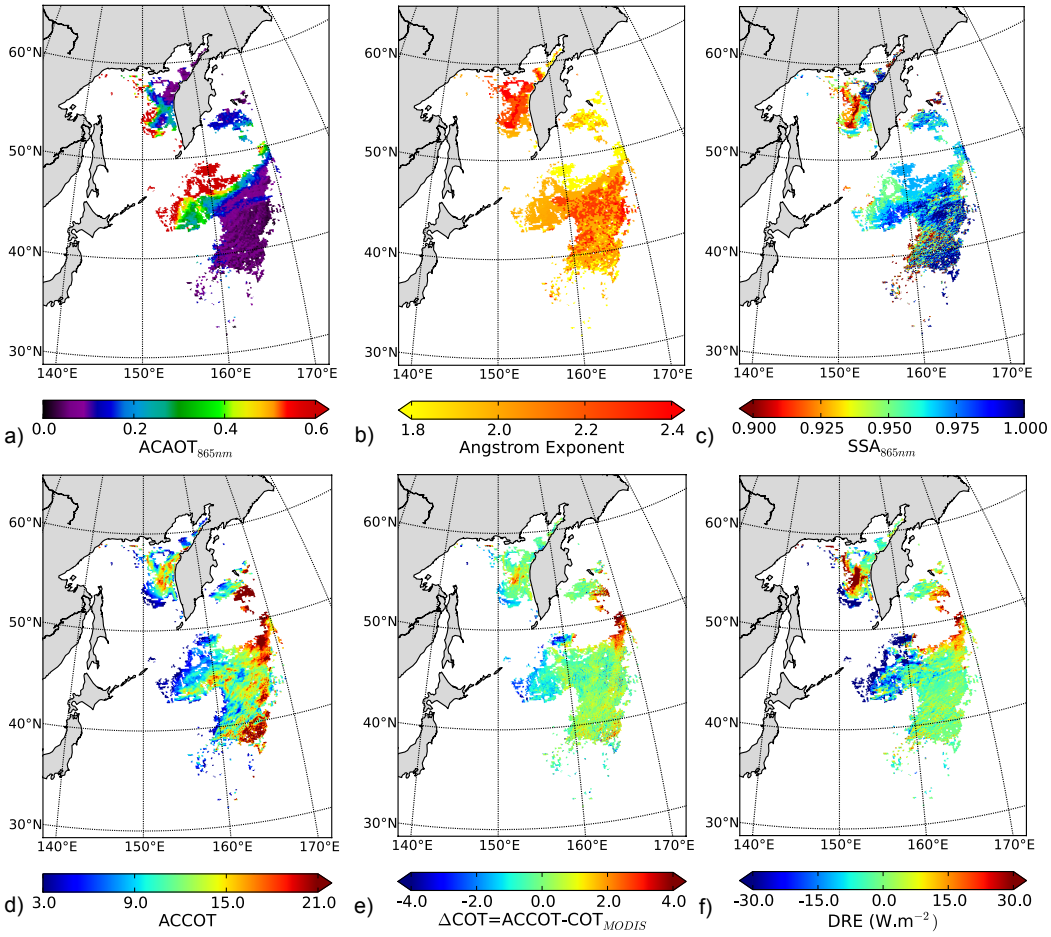

Figure 8. Same as Fig. 7 for biomass burning aerosols from Siberia on 3rd July 2008.

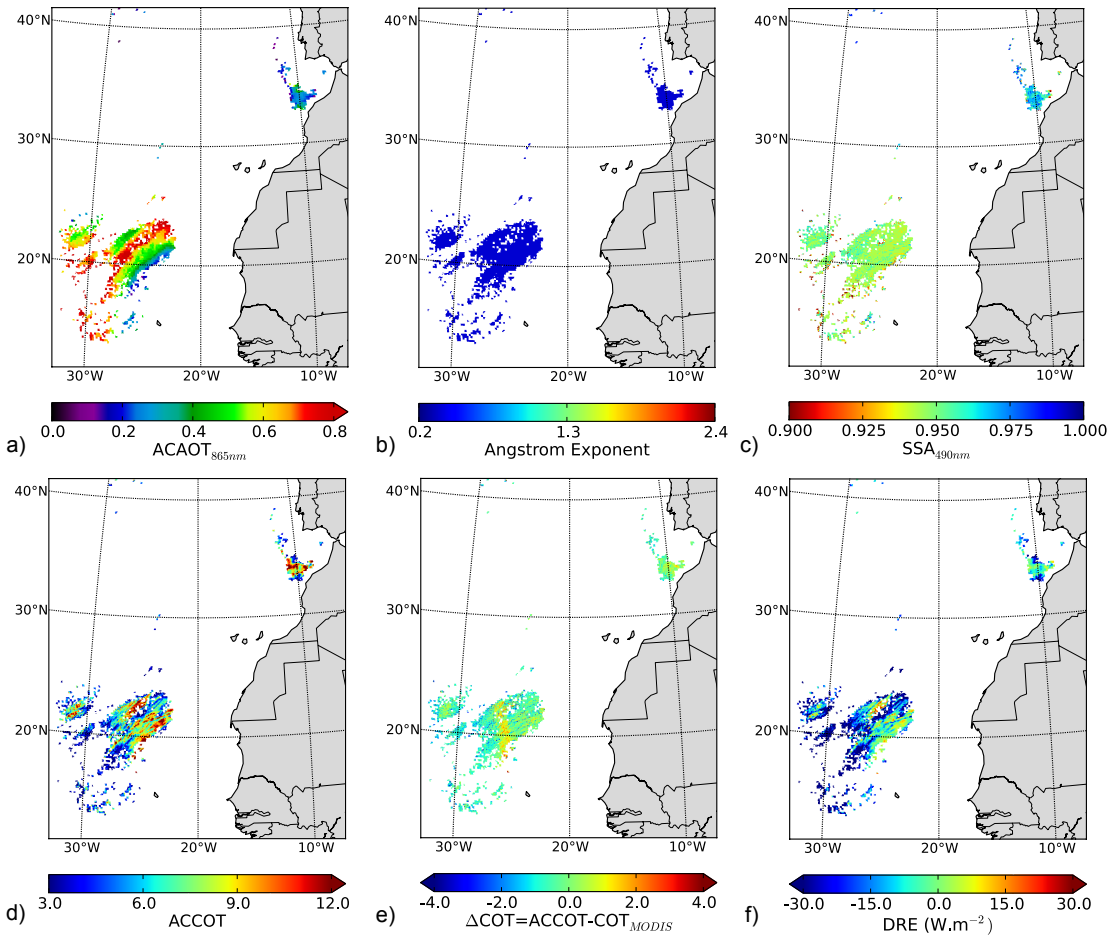

Figure 9. Same as Fig. 7 for Saharan dust above clouds on 4th August 2008, except Fig. 9c that displays the aerosol SSA at 490 nm.

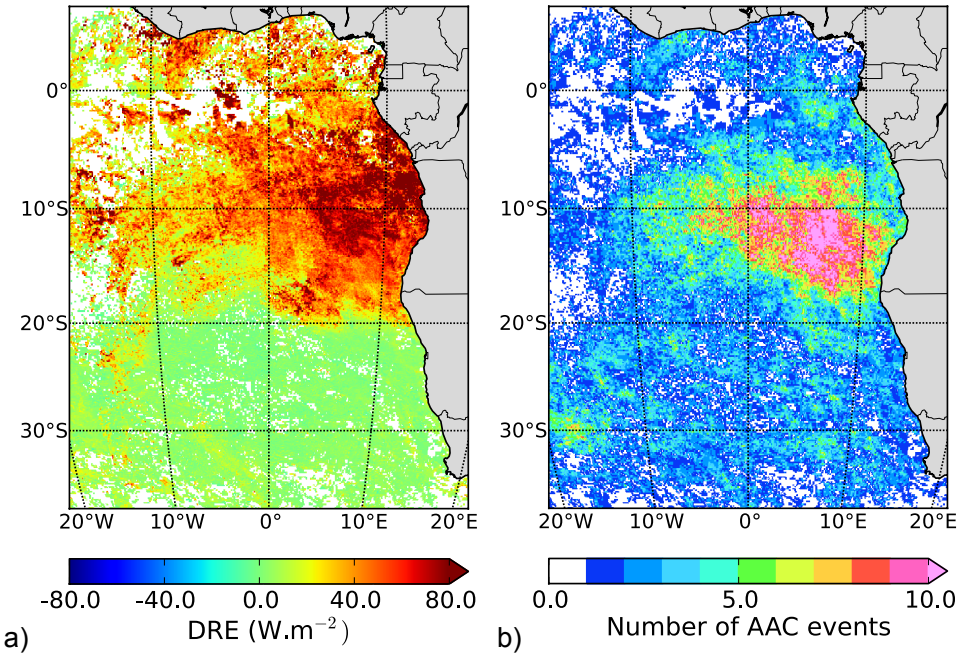

Figure 10. Direct Radiative Effect of aerosols above clouds averaged through August 2006 (a) and number of associated events (b). The DRE has been processed over scenes with a Cloud Fraction (CF) equal to 1 and COT ≥ 3.

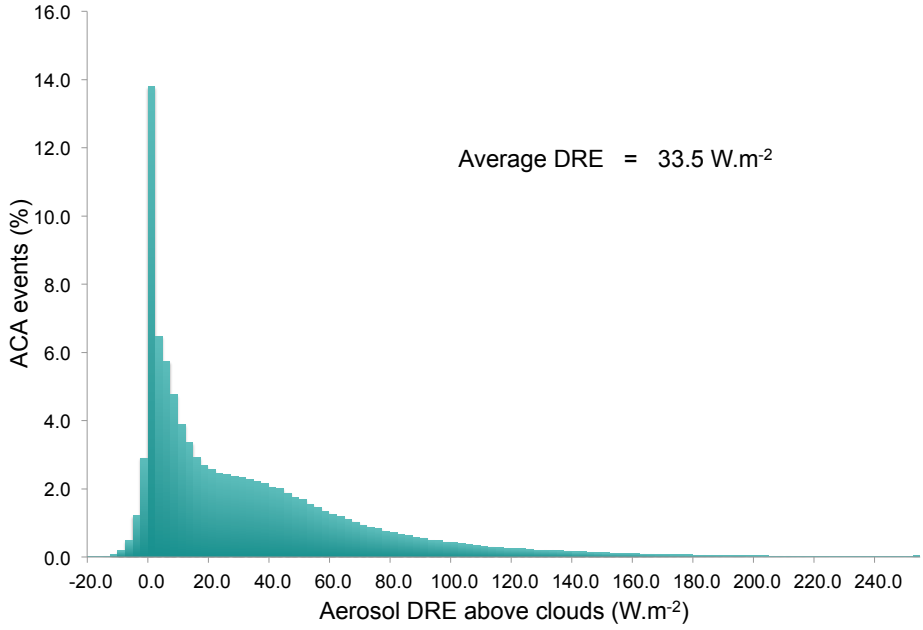

Figure 11. Frequency distribution of the aerosol Direct Radiative Effect above clouds for August 2006 for the South East Atlantic Ocean. Only scenes with COT ≥ 3 and CF = 1 are considered.

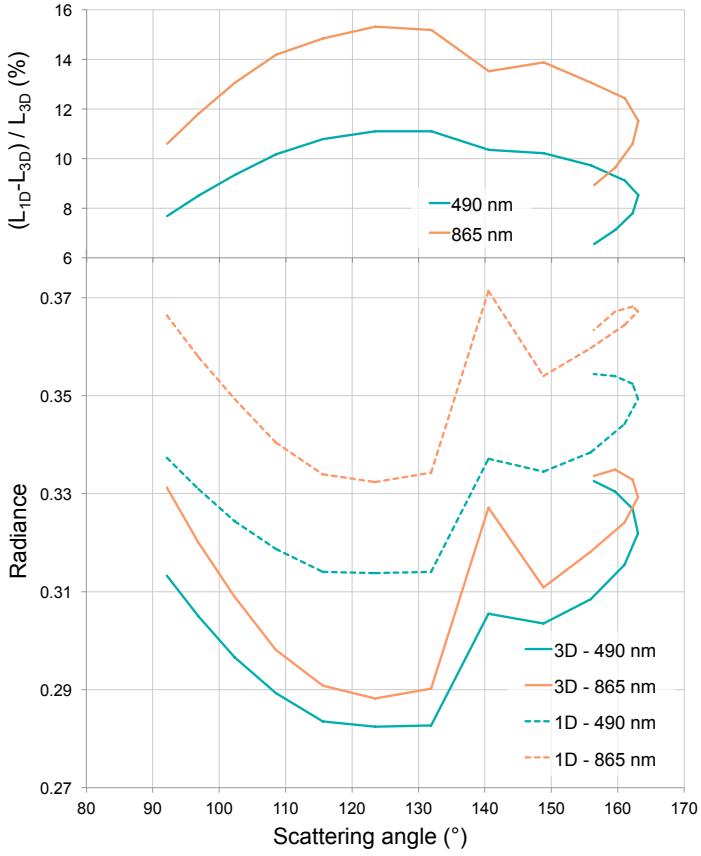

Figure 12. Simulated radiances for aerosols above a heterogeneous cloud (σ(COT)/COT = 0.6) at 490 nm (green lines) and 865 nm (orange lines) for a solar zenith angle of 40°. 3D signals (continuous lines) have been obtained thanks to the 3DMCPOL code and based on a cloud field modeled with 3DCLOUD.